

A freely moving body in a boundary layer: nonlinear separated-flow effects

Frank Smith^a, Ryan Palmer^a

a. Department of Mathematics, University College London, Gower Street, London, WC1E 6BT, UK.

Corresponding author: Frank Smith, f.smith@ucl.ac.uk

Keywords: fluid-body interaction, modelling, analysis, ice particles

Abstract.

In the boundary layer of fluid on a moving solid surface (such as on a moving vehicle e.g. ships) a thin body is translating parallel to the surface. The streamwise movement of the body relative to the solid surface is substantial, with the upstream or downstream velocity being comparable with the free-stream velocity. The dynamic fluid/body interaction here incorporates the effects of incident vorticity, nonlinear and separating flow. Modelling, analysis and reduced computation explore the all-important influences of body shape, moment of inertia and centre-of-mass location. These influences and the initial conditions affect whether nonlinear oscillations of the fluid and body motions continue or fully nonlinear focussing occurs after a finite time.

1. Introduction.

Of interest in this paper is the understanding and prediction of the motion of a body near the solid surface of a transport vehicle, or other moving solid surface, so near that the body lies within the comparatively thin boundary layer of fluid flow on the vehicle. The feedback effect of the body motion on the fluid flow is also of concern. The typical Reynolds number involved is large in the many relevant applications [1-14]. Sea-ice applications concern the hazard posed by ice shards or lumps impacting upon ships, submerged vessels, installations or their interaction with ice floes. Aircraft-ice applications are likewise for ice particles but impacting upon a fuselage, wing, blade or engine inlet. In addition there are a number of other application areas (for example food-sorting) that motivate explorations of dynamic fluid/body interactions.

Modelling, analysis and allied computation provide the focus of study here. There is a series of such studies for oncoming uniform flow in [1-5]; in effect these cases correspond to the body lying outside the original boundary layer and so have negligible vorticity in the resulting fluid/body interaction. These include studies of multiple bodies in channels or ducts concerned with the modelling of food-sorting, as well as particle-skimming on water, related entry and exit phenomena, liftoff of a body from a solid surface, and flooding and sinking of submerged bodies. In contrast with [1-5] the present study allows for substantial vorticity by virtue of the oncoming boundary layer velocity profile with no slip at the underlying solid surface or wall. Recent works also allowing for oncoming nonzero vorticity are in [6, 7] concerned with boundary layers and channel flows. We should note in addition a number of intriguing direct-computational investigations and experiments described in [5, 8-14] over various different parameter ranges.

Nonzero velocity of the solid body in the streamwise direction relative to the wall is believed to be a potentially important factor in the evolving fluid/body interplay and it is addressed in the current investigation. This is as opposed to the assumption in [1-6] of zero relative velocity. A suggestion in [7] points to considerable changes taking place in the fluid flow and body motion when the relative velocity is increased from zero, and the current paper follows that suggestion through in detail. An assumption of quasi-inviscid fluid flow is consistent with the above suggestion and this is used here to shed light on the effects of nonlinearity and in particular separation or reversal of the fluid flow when interacting with the moving body. In view of the fact that the previous studies [6, 7] concentrate on linear properties the present treatment of nonlinear and separating-flow effects represents a new aspect.

The body, if thin and at sufficiently small incidence, can move with constant velocity in the streamwise direction inside the boundary layer under a free stream because the forces in that direction are generally small compared with the mass-acceleration contributions in the same direction. This applies over a wide

range of conditions [1-7]. Further, if the velocity of the body relative to the wall is negative when measured in the streamwise direction then, relative to the body, we have a downstream-moving wall and a corresponding incident velocity profile which is positive at the wall. Conversely a downstream-moving body is associated with an upstream-moving wall in a coordinate frame moving with the body of course. See also [15-18]. Both scenarios are of concern.

In producing this article, we have three main motivating examples in mind (amongst several avenues of interest) that relate to the hydrodynamics of ice. Two relate to the coupled movement of sea ice and aquatic vehicles, such as ships and boats. In the first configuration, the vehicle is moving through the body of water whereupon a piece of ice traverses alongside it, floating on the water surface. Here the lump interacts with the developing boundary layer along the side of the vehicle. The second scenario is similar, however now the lump of ice is submerged and traverses the underside of the hull, interacting with the boundary layer there. The third scenario relates to aircraft icing, which is a significant topic in aviation safety. Whilst cruising at high altitudes aircraft may be impacted by atmospheric ice crystals leading to the formation of ice on wings, fuselages and vital components such as engines and pitot tubes. In turn this can degrade the performance of the aircraft and at worst result in a system failure. The following analytical investigations provide physical insight for the above scenarios. They provide key details for understanding the underlying mechanisms that govern the development and structure of the fluid flow, and that determine the trajectory and potential impact of a piece of ice on a moving surface.

The sections to come are as follows. Section 2 sets the scene for the fluid/body interaction of interest in nondimensional terms with a large Reynolds number Re based on the original flow development length. The body in question, which is taken to be thin and nearly aligned with the incident boundary-layer flow, is moving upstream or downstream with uniform $O(1)$ streamwise velocity u_c relative to the wall or ground, within the core of an $O(Re^{-1/2})$ thick boundary layer. Laminar two-dimensional unsteady flow of an incompressible fluid of constant density is explored. The densities of the fluid and the solid body are $\check{\rho}_F, \check{\rho}_B$ where the “check” denotes a dimensional quantity. The representative streamwise length of the boundary layer is written \check{l} , for example its development length. We work in a non-dimensional form with velocity components (u, v) , pressure variation p , Cartesian coordinates (x, y) and time t based on $\check{u}, \check{\rho}_F, \check{u}^2, \check{l}$ and \check{l}/\check{u} respectively. The dimensional mass is written $\check{\rho}_B \check{\alpha}_B M_N$, with M_N being nondimensional and with $\check{\alpha}_B$ standing for the cross-sectional area of the two-dimensional body, and similarly the nondimensional moment of inertia is written I_N . Section 3 addresses reduced body speeds where the nonlinear effects persist and so flow separation can occur. Computational solutions and analytical features are described in sections 4 and 5 respectively. A discussion of the results is presented in section 6. Section 7 presents further comments and conclusion.

2. Interaction in a boundary layer.

The fluid/body interaction takes place with the relative velocity of the body $u_c = C$ being of order unity and with a single thin body within the boundary layer. Mainly we consider negative C values and so we put $C = -D$ where the constant D is positive; we discuss positive C values later on. See figure 1. The flow behaviour is quasi-inviscid for the most part although it is worth noting that there is a connection with recent viscous/inviscid work in [7] as their assumed small streamwise velocity increases. We expect the pressure variation p in the gap between the body under-surface and the wall, and the streamwise velocity component u , to all be of order unity. Also, the normal velocity component v in the oncoming boundary layer is smaller, having the classical scaling of order Δ where $\Delta = Re^{-1/2}$. The interactive effects here are expected to cover the whole boundary layer and to be influenced by the whole incident velocity profile $u = u_0(Y)$ of the boundary layer over the fixed solid plane wall, with $u_0(0) = 0$, because of no slip at that wall and the scaled skin friction constant $\lambda = u'_0(0) > 0$. That is ahead of the body.

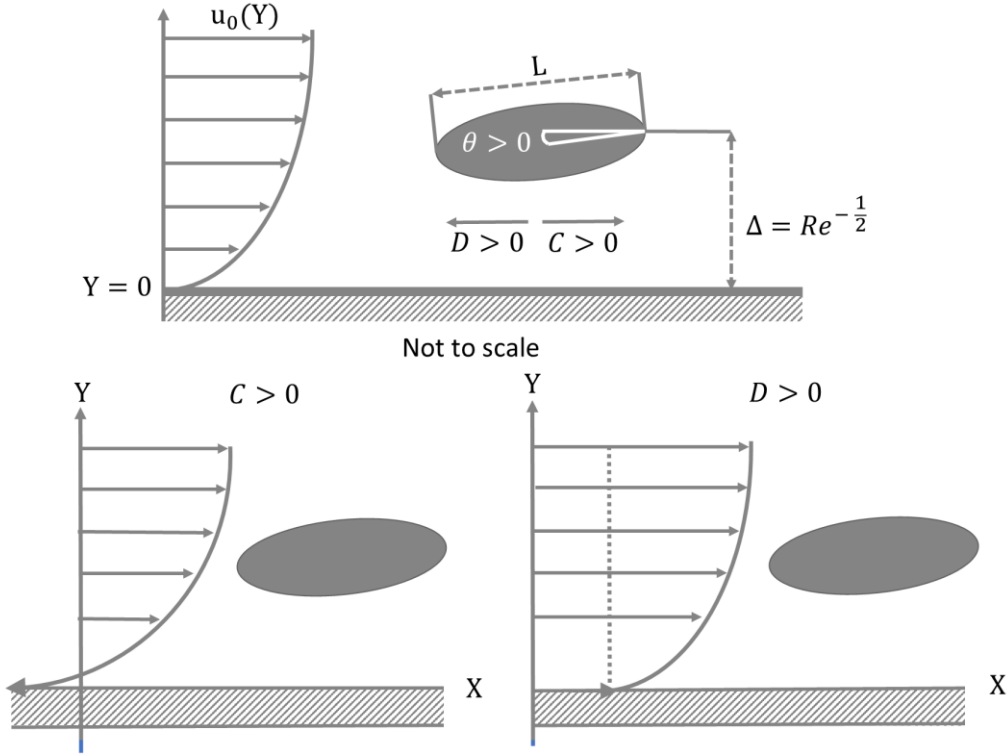


Figure 1. The fluid/body configuration with, in the upper diagram, the body translating upstream or downstream at uniform speed relative to the wall. The lower diagrams are drawn in a coordinate frame moving with the body. (The sketches are not to scale.) Here $u_0(Y)$ is the incident velocity profile in the boundary layer and L, Δ are nondimensional length scales.

Continuing this work in a frame moving streamwise with the body, it is implied that the incident flow upstream (ahead of the Euler zone described below) has an effective velocity profile $u_0(Y) + D$, hence the incident fluid motion is forward at the wall (when D is positive) and is taken to be forward across the entire boundary layer.

The appropriate coordinate scalings here for the interaction between the fluid flow and the body are $x = LX, y = \Delta Y$ where L is the body length as shown in the sketch in figure 1. The body length is assumed to satisfy $\Delta \ll L \ll 1$, meaning that the body is long compared with the thickness of the incident boundary layer and short relative to the development length of the boundary layer. The body occupies $0 < X < 1$ and is supposed to be of thickness $O(\Delta)$ such that there is a fluid gap of thickness $O(\Delta)$ between the body and the wall $Y = 0$. The time scale is such that $t = \sigma T$ where the constant σ is the typical translation time along the body, which is of order L , and T is of order unity. Thus the scaled governing equations for the fluid motion in the gap give the nonlinear unsteady inviscid system:

$$u_X + V_Y = 0, \quad u_T + uu_X + Vu_Y = -p_X \quad (2.1a,b)$$

with the unknown scaled pressure $p = p(X, T)$ being independent of Y from the normal momentum balance. Here $v = L^{-1} \Delta V$ to leading order with V being of order unity. The system is subject to a kinematic boundary condition (2.2a), a tangential flow requirement (2.2b), an incident profile condition (2.2c), a Kutta effect (2.2d) and the unknown body movement (2.2e, f):

$$V = F_T + uF_X \text{ at } Y = F(X, T) = f_u(X) + h(T) + (X - \beta)\theta(T), \quad (2.2a)$$

$$V = 0 \text{ at } Y = 0, \quad (2.2b)$$

$$p = 0, \quad u = w_0(Y) \text{ given at } X = 0_- \text{ but } p = p^+, \quad u = w_0^+(Y) \text{ at } X = 0_+, \quad (2.2c)$$

$$p = 0 \text{ at } X = 1, \quad (2.2d)$$

$$\text{and } Mh_{TT} = \int_0^1 p \, dX, \quad I\theta_{TT} = \int_0^1 (X - \beta) p \, dX. \quad (2.2e, f)$$

Commenting further on these conditions, we remark first that it is an Euler effect that leads to (2.2c) where the upstream conditions at $X = 0_-$ are prescribed but the pressure p^+ and velocity profile $w_0^+(Y)$ at $X = 0_+$ are to be determined (as explained shortly). The centre of mass of the body is assumed to be at the midway station $X = \beta$, $0 < \beta < 1$. The normalised height h of the centre of mass and the angle θ of inclination of the body centre-line curve are scaled on Δ , while M, I are the scaled mass and moment of inertia as in (2.3) below. The incident velocity profile ahead of the body in this frame is $w_0 = u_0 + D$: the relation between the profiles w_0, w_0^+ is explored below, and we observe that $w_0(0) = D$ is prescribed. The underbody shape $f_u(X)$ relative to the body centre-line curve is independent of time T and is taken such that $f_u(0) = f_u(1) = f_0$ for convenience and without loss of generality, where f_0 is a given positive constant. The Kutta condition (2.2d) at the trailing edge of the body is as in [1-7]. (We remark in passing that the assumption of $\Delta \ll L$ implies the body cannot rotate sufficiently to change the body length from unity and so the Kutta condition is always applied at $X = 1$.) It is notable that unsteadiness appears in both the fluid and the body equations, contrasting with [6, 7]. The presence of nonzero vorticity is also noteworthy, entering because of the non-uniform incident flow in (2.2c). Moreover, the pressure on the top surface of the body is equal to the local free-stream pressure which is here taken to be zero for convenience: the unknown pressure in (2.1a)-(2.2f) is the excess pressure in the gap. (The flow on top of the body is as in [7], and further relatively thin viscous layers are present on the body surface and on the wall.) Finally here, we remark that the nonlinear system is basically the same as in [1] except for the incident nonzero vorticity ($dw_0/dY, dw_0^+/dY$) in the current scenario.

The scaling requirements on the body mass M_N and moment of inertia I_N stem from the physical balances in (2.2e, f) and are, on the mass,

$$M_N \sim M \frac{\check{\rho}_F L^2}{\check{\rho}_B \Delta^2}. \quad (2.3)$$

Here the dimensional cross-sectional area \check{a}_B of the body is taken to be $\check{l}^2 L \Delta$ as a representative value. It is supposed that I, M are both of the same $O(1)$ order of magnitude here.

The relation between the velocities w_0 ahead of the body and w_0^+ in the gap entry depends on the unknown pressure jump from zero incident pressure upstream (at $X = 0_-$) to p^+ downstream (at $X = 0_+$) across the Euler region wherein x, y are both $O(\Delta)$. Here $p^+ = p(0_+, T)$ is unknown in advance. The governing equations in that region are the quasi-steady Euler equations, which lead to conservation of vorticity and conservation of the Bernoulli property $p + 1/2 (u^2 + v^2)$ along streamlines of constant ψ passing through the region. The quasi-unidirectional flow profiles at $X = 0 \pm$ are therefore related by

$$Y = \int_0^1 w_0(\eta) \left[(w_0(\eta))^2 - 2p^+ \right]^{-1/2} d\eta. \quad (2.4a)$$

as far as the mapping of coordinates from z upstream to Y downstream is concerned for a given streamline. See appendix A. The result (2.4a) is valid for completely *forward flow*. From (2.4a) we can also determine the velocity profile $w_0^+(Y)$ as $d\psi/dY$, whereas upstream $w_0(z)$ is $d\psi/dz$, as shown in figure 2 for the sample profile $u_0(z) = z + 1 - \exp(-z)$. In figure 2(a), the velocity profiles w_0, w_0^+ are plotted in terms of Y just prior to ($X = 0_-$) and just after ($X = 0_+$) the Euler region, while ψ gives the stream function. In this example the relative translational velocity D is 0.7 and the pressure rise p^+ is 0.2 as a motivational case. See (2.4a-c). Figure 2(b) is as in figure 2(a) except that the vertical coordinate z upstream is also shown for comparison and this example has $D = 0.1$, $p^+ = 0.3D^2$, again to provide motivation for subsequent study. Figure 2(c) is for $D = 0.1$ (black, magenta, cyan curves) and 0.05 (yellow, grey) with $p^+ = 0.3D^2$ for comparison purposes; the cases in figures 2(b,c) are in anticipation of the scalings investigated subsequently in the section 3. Additionally we have

$$w_0^+(0) = D^+ \text{ where } D^{+2} = D^2 - 2p^+. \quad (2.4b)$$

in view of the Bernoulli property. Here D^+ is defined as the positive square root, $+(D^2 - 2p^+)^{1/2}$. Thus $w_0^+(0) > 0$ in the case of forward flow. Moreover the wall where Y is zero corresponds to ψ zero. The formula (2.4a) enables the effective captured mass flux ψ to be found at the leading edge of the body undercarriage in terms of a guessed p^+ , for a prescribed input w_0 , at least if the Y value of the leading edge is known at any particular instant T . This, when combined with (2.2a,b), allows the gap-flow solution to be determined progressively from the leading edge to the trailing edge station. Hence the Kutta condition (2.2d) applied at the latter station can act to yield a condition to pin down the p^+ guess. The spatially elliptic nature of the flow problem for $0 < X < 1$ stands out.

If the velocity profile at $X = 0_+$ becomes *partially reversed* for an extent $0 < Y < Y_0$ say, where Y_0 is in general time-dependent but acts as if constant as far as the local jump conditions are concerned, then an extra displacement takes place. This is across the Euler zone due to eddy formation and is such that (2.4a) is altered to

$$Y = \int_0^z w_0(\eta) \left[(w_0(\eta))^2 - 2p^+ \right]^{-1/2} d\eta + Y_0. \quad (2.4c)$$

The wall streamline upstream at $X = 0_-$ continues forward into the dividing streamline at height Y_0 . Underneath the latter the velocity profile $w_0^+(Y)$ in $0 < Y < Y_0$ is not determined so directly by the incident profile w_0 but we suppose that it is a smooth continuation of the profile holding for $Y > Y_0$. (Discontinuities might be admissible over the present length scales in some circumstances but we shall seek a smooth form here.) The property (2.4b) continues to hold since the streamlines of the reversed-flow part of the eddy become those of the forward-flow part; here however the value $-D^+ < 0$ is the appropriate root because of the reversed flow at the wall. In the example of incident uniform shear $w_0(z) = \lambda z + D$ the resulting profile $w_0^+(Y)$ is $\lambda(Y - Y_0) + D^+$ for $Y \geq Y_0$ to preserve vorticity. Using continuation and the result that $w_0^+(0) = -D^*$ then gives $Y_0 = 2D^+/\lambda$ as the dividing streamline position.

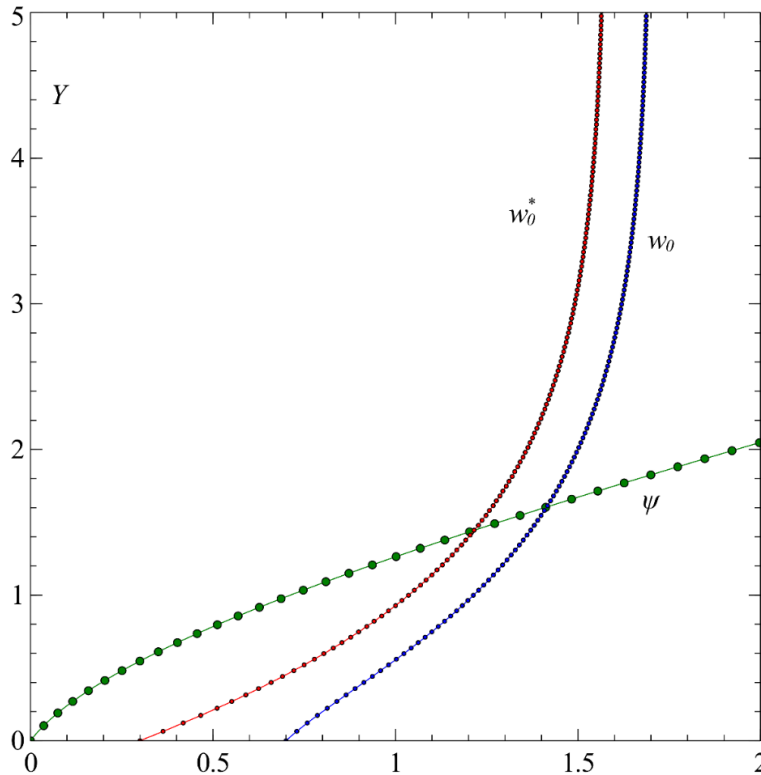


Figure 2a. Velocity profiles w_0 , w_0^+ in terms of Y just prior to ($X = 0_-$) and just after ($X = 0_+$) the Euler region, with stream function ψ . Relative velocity and pressure rise are $(D, p^+) = (0.7, 0.2)$.

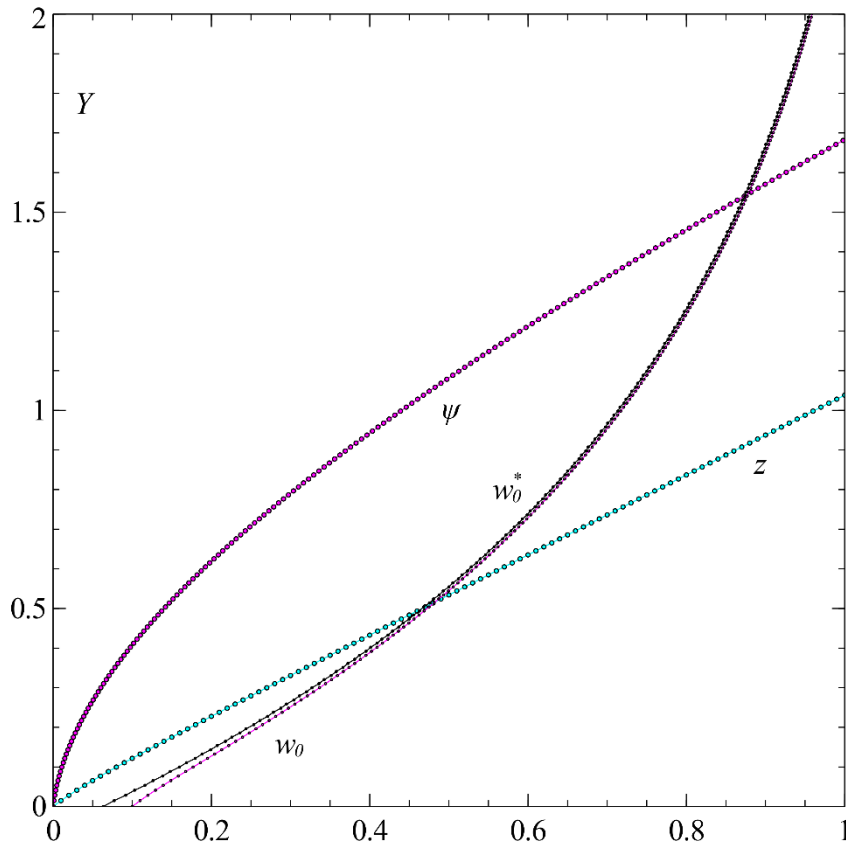


Figure 2b. As in (a) but with normal coordinate z upstream shown for comparison, where $(D, p^+) = (0.1, 0.3D^2)$.

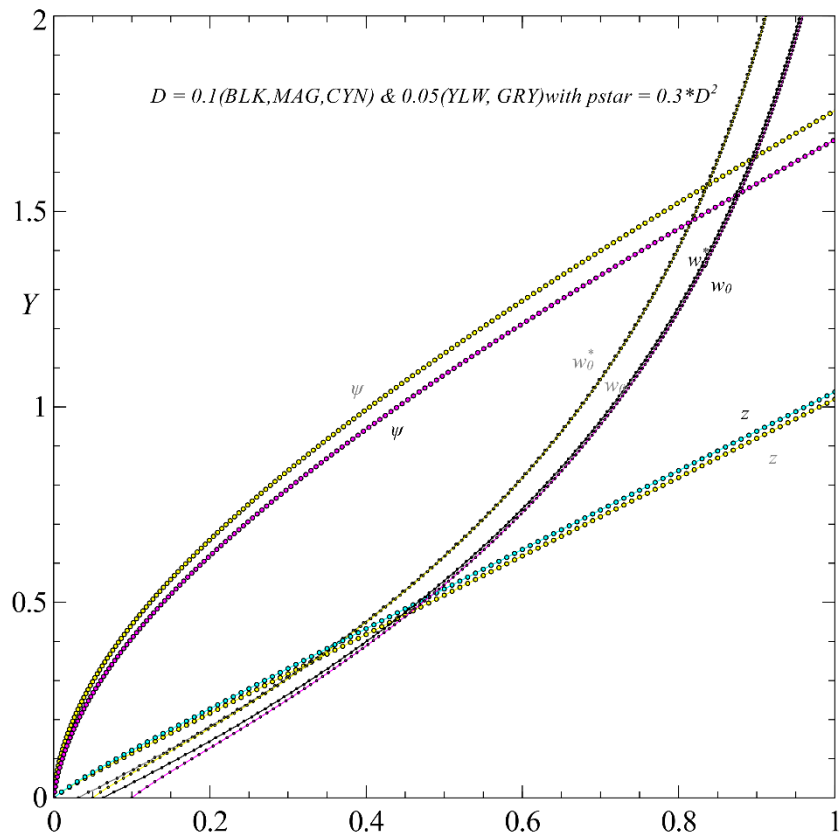


Figure 2c. As (b) but compared with $(0.05, 0.3D^2)$.

3. Nonlinear effects at reduced body speeds.

The question now arises of: what occurs if the relative wall velocity D is small? Suppose the incoming flow has $D = \varepsilon \bar{D}$ with the uniform parameter ε small and \bar{D} of order unity. We then expect to have typical p^+ small, say $p^+ = \varepsilon^2 \bar{p}^+ + \dots$, and from (2.4a-c) the response $D^+ = \varepsilon \bar{D}^+ + \dots$ with $\bar{D}^+ = (\bar{D}^2 - 2\bar{p}^+)^{1/2}$ being the positive square root. Two flow regions are induced in the gap as follows, subject to assuming the X scale remains comparable with the body length of $O(1)$ and the body shape is comparatively thin, i.e. f_u is equal to the constant f_0 to within an $O(\varepsilon)$ perturbation. Here the initial velocity profile $w_0^+(Y)$ in the gap becomes $u_0(Y) + O(\varepsilon)$ for the majority of the gap flow as described in Appendix A and as found in figure 2(c), where the $O(\varepsilon)$ term is a displacement effect proportional to $u_0'(Y)$. There is also a crucial sublayer arising at small Y values. Subsections 3.1 and 3.2 below consider the two flow regions in turn followed by (c), (d) on the consequent dynamics.

3.1. The majority or bulk.

In the majority of the fluid:

$$u = u_0(Y) + \varepsilon(\pm \bar{D}^+ + u_1) + \dots, \quad V = \varepsilon v_1 + \dots, \quad p = \varepsilon^2 p_1 + \dots, \quad \text{for } Y \text{ of } O(1). \quad (3.1a-c)$$

with time $T = \varepsilon^{-1} \bar{T}$ being relatively slow. See Appendix A regarding the \bar{D}^+ contribution in (3.1a). We note that $u_0(Y)$ is zero at the wall and so we can expect $u_1(0_+, 0, \bar{T})$ to be zero as well. The \pm sign on \bar{D}^+ is as described near the end of section 2 as well as in (3.3d) below. The time scale and the pressure size in (3.1c) are inferred from the form in subsection 3.2 below. Substitution into (2.1) gives us the quasi-steady linear response

$$u_{1X} + v_{1Y} = 0, \quad u_0(Y) u_{1X} + v_1 u_0'(Y) = 0, \quad (3.2a,b)$$

to leading order. So the flow suffers an unknown negative displacement $A_1(X, \bar{T})$ such that

$$u_1 = A_1(X, \bar{T}) u_0'(Y), \quad v_1 = -A_{1X}(X, \bar{T}) u_0(Y). \quad (3.3a,b)$$

The prime denotes the derivative with respect to Y . The behaviour in (3.3a, b) is consistent with the requirement (2.2a) provided that

$$A_1(X, \bar{T}) = -\bar{h}(\bar{T}) - (X - \beta) \bar{\theta}(\bar{T}) - \bar{f}_u(X) + \bar{K}(\bar{T}). \quad (3.3c)$$

The essential Kutta function \bar{K} is an unknown function of time \bar{T} ; and also we have used $[h, \theta, F, f_u] = [0, 0, f_0, f_0] + \varepsilon [\bar{h}, \bar{\theta}, \bar{F}, \bar{f}_u] + O(\varepsilon^2)$ scaled appropriately. The other original conditions (2.2b-f) remain to be addressed later on. Also, we have that

$$\bar{K}(\bar{T}) = \bar{h}(\bar{T}) - \beta \bar{\theta}(\bar{T}) - \lambda^{-1} \{ \bar{D} - \bar{D}^+ \} - \bar{Y}_0, \quad ,$$

from comparing (3.3c) with the jump conditions (2.4a,c): see Appendix A which shows that $Y_0 = \varepsilon \bar{Y}_0 = 2\varepsilon \bar{D}^+$ to leading order with flow reversal as opposed to forward flow which has \bar{Y}_0 being zero. The above can thus be written conveniently as

$$\bar{K}(\bar{T}) = \bar{h}(\bar{T}) - \beta \bar{\theta}(\bar{T}) + \lambda^{-1} \{ \pm \bar{D}^+ - \bar{D} \}, \quad (3.3d)$$

for the totally forward and partially reversed cases respectively. Once we know \bar{p}^+ then, for given $\bar{h}, \bar{\theta}$ values, the result (3.3d) determines \bar{K} explicitly.

3.2. Near the solid wall.

A sublayer is induced in which the pressure, being independent of Y , is as in (3.1c) but the velocities have

$$u = \varepsilon(\pm \bar{D}^+ + \bar{u}) \dots, \quad V = \varepsilon^2 \bar{V} + \dots, \quad \text{for } Y = \varepsilon \bar{Y}. \quad (3.4a,b)$$

Here we obtain from (2.1) the nonlinear unsteady flow equations

$$\bar{u}_X + \bar{V}_Y = 0, \quad \bar{u}_T + (\pm \bar{D}^+ + \bar{u})\bar{u}_X + \bar{V}\bar{u}_Y = -p_{1X}, \quad (3.5a,b)$$

which are subject to

$$\bar{V} = 0 \text{ at } Y = 0, \quad \bar{u} \sim \lambda \bar{Y} + \lambda A_1 \text{ as } \bar{Y} \rightarrow \infty, \quad (3.5c,d)$$

from (2.2b) and from matching with (3.1a, b) in turn. The complete solution here (see also [19]) is simply

$$\bar{u} = \lambda \bar{Y} + \lambda A_1, \quad \bar{V} = -\lambda \bar{Y} A_{1X}, \quad (3.5e,f)$$

provided that from substitution into (3.5a, b) the functions A_1, p_1 are related by

$$\lambda A_{1\bar{T}} + \lambda(\pm \bar{D}^+ + \lambda A_1)A_{1X} = -p_{1X}. \quad (3.5g)$$

We find that this form agrees with that in [7] for the steady case when u_c is smaller. Unlike in [7] both the scaled pressure p_1 and the scaled uniform velocity \bar{D} are discontinuous across the leading-edge station $X = 0$, as is A_1 which is discontinuous in general because of the response (3.3c). Thus we have the two requirements

$$p_1 = \bar{p}^+ \text{ at } X = 0_+, \quad p_1 = 0 \text{ at } X = 1, \quad (3.6a,b)$$

on the main pressure response p_1 , with $\bar{p}^+(\bar{T})$ to be found.

The remaining equations for determining A_1, p_1 come from the body-motion balances in (2.2e,f). These yield

$$\bar{M} \bar{h}_{\bar{T}\bar{T}} = \int_0^1 p_1 dX, \quad \bar{I} \bar{\theta}_{\bar{T}\bar{T}} = \int_0^1 (X - \beta) p_1 dX, \quad (3.7a, b)$$

where $(\bar{M}, \bar{I}) = \varepsilon (M, I)$ are assumed to be of $O(1)$ with respect to ε . We thus have four equations (3.3c), (3.5g), (3.7a,b) for $A_1, p_1, \bar{h}, \bar{\theta}$ spatially in effect along with temporal conditions (3.6a,b).

3.3. Interaction equations.

From (3.5g), making use of (3.3c) and writing $\bar{K}_{\bar{h}} = \bar{K} - \bar{h}$, we obtain

$$-\frac{p_{1X}}{\lambda} = \dot{\bar{K}}_{\bar{h}} - (X - \beta)\dot{\bar{\theta}} + \lambda\{\phi + [(X - \beta)\bar{\theta} + \bar{f}_u(X)]\{\bar{\theta} + \bar{f}'_u(X)\}, \quad (3.8a)$$

where the function $\phi = -(\bar{K}_{\bar{h}} \pm \bar{D}^+)/\lambda$. Hence integration in X gives, with unknown function $E_1(\bar{T})$,

$$-\frac{p_1}{\lambda} = \dot{\bar{K}}_{\bar{h}} X - \left(\frac{1}{2} X^2 - \beta X\right) \dot{\bar{\theta}} + \frac{\lambda}{2} \{\phi + [(X - \beta)\bar{\theta} + \bar{f}_u(X)]\}^2 + E_1(\bar{T}). \quad (3.8b)$$

Now condition (3.6a) imposed at the leading edge requires

$$E_1(\bar{T}) = -\frac{\bar{p}^+}{\lambda} - \frac{\lambda}{2} \{\phi - \beta\bar{\theta}\}^2. \quad (3.9a)$$

since \bar{f}'_u is zero at the leading edge. Similarly the Kutta condition (3.6b) at the trailing edge leads to

$$E_1(\bar{T}) = -\dot{\bar{K}}_{\bar{h}} - \frac{\lambda}{2} \{\phi + (1 - \beta)\bar{\theta}\}^2 + \left(\frac{1}{2} - \beta\right) \dot{\bar{\theta}}. \quad (3.9b)$$

Note that for $\beta = 0.5$ the $\dot{\bar{\theta}}$ disappears. Elimination of $E_1(\bar{T})$ therefore gives us

$$-\dot{\bar{K}}_{\bar{h}} - \frac{\lambda}{2} \{\phi + (1 - \beta)\bar{\theta}\}^2 + \left(\frac{1}{2} - \beta\right) \dot{\bar{\theta}} = -\frac{\bar{p}^+}{\lambda} - \frac{\lambda}{2} \{\phi - \beta\bar{\theta}\}^2. \quad (3.10a)$$

and so from the definition of ϕ we find the nonlinear equation

$$\dot{\bar{K}}_{\bar{h}} - (\lambda \bar{K}_{\bar{h}} \pm \bar{D}^+) \bar{\theta} = \frac{\bar{p}^+}{\lambda} + \left(\frac{1}{2} - \beta\right) \dot{\bar{\theta}} - \lambda \left(\frac{1}{2} - \beta\right) \bar{\theta}^2. \quad (3.10b)$$

linking $\bar{K}_{\bar{h}}, \bar{\theta}, \bar{p}^+$.

Meanwhile substituting (3.8b) into the body-motion equations (3.7a,b) gives two equations between $\bar{\theta}, \bar{K}_{\bar{h}}$ and \bar{p}^+ and \bar{h} ; so that makes three equations so far. The other two equations are the definition of the relative lateral distance $\bar{K}_{\bar{h}} = \bar{K} - \bar{h}$ from the previous paragraph and the Euler jump effect from Appendix A, namely (3.3d) between $\bar{\theta}, \bar{K}_{\bar{h}}$ and \bar{p}^+ . Thus we have 5 equations for the 5 unknowns $\bar{\theta}, \bar{K}_{\bar{h}}, \bar{p}^+, \bar{K}$ and \bar{h} as functions of \bar{T} .

3.4. Governing equations for a parabolic underbody shape.

A useful basic case is the constant-curvature underbody for which

$$\bar{f}_u(X) = bX(1-X) \text{ for } 0 < X < 1. \quad (3.11b)$$

Here b is a given positive or negative constant. So now (3.8b) yields the pressure distribution

$$p_1 = \sum_{n=0}^4 \pi_n X^n, \quad (3.12a)$$

where the coefficients are time-dependent, being

$$\pi_0 = \bar{p}^+ \quad (3.12b)$$

$$\pi_1 = -\lambda \dot{\bar{K}}_{\bar{h}} - \beta \lambda \dot{\bar{\theta}} - \lambda^2 (\phi - \beta \bar{\theta}) (\bar{\theta} + b), \quad (3.12c)$$

$$\pi_2 = \frac{1}{2} \lambda \dot{\bar{\theta}} - \frac{\lambda^2}{2} \{-2b(\phi - \beta \bar{\theta}) + (\bar{\theta} + b)^2\}, \quad (3.12d)$$

$$\pi_3 = \lambda^2 b (\bar{\theta} + b), \quad (3.12e)$$

$$\pi_4 = -\frac{\lambda^2}{2} b^2. \quad (3.12f)$$

Hence the body-motion balances take on the explicit forms

$$M \ddot{\bar{h}} = \sum_{n=0}^4 (n+1)^{-1} \pi_n, \quad (3.13a)$$

$$I \ddot{\bar{\theta}} = \frac{1}{2} \sum_{n=1}^4 n(n+1)^{-1} (n+2)^{-1} \pi_n. \quad (3.13b)$$

and we have four equations for $\bar{\theta}, \bar{K}, \bar{h}, \bar{p}^+$ namely (3.13a,b) with (3.10b), (3.3d). We recall that in (3.3d) \bar{D} is a prescribed positive constant. As far as conveniently calculating solutions is concerned however, say for time-marching, we can first see three equations (3.13b), (3.10b), (3.3d) for $(\bar{\theta}, \bar{K}_{\bar{h}}, \bar{p}^+)(\bar{T})$ and secondly one equation (3.13a) for $\bar{h}(\bar{T})$. In that sense the angular momentum balance (3.13b) dominates over the normal momentum balance (3.13a). The three equations (3.13b), (3.10b), (3.3d) effectively represent the body motion, the fluid motion and the pressure conditions respectively; the three unknowns themselves dictate how much of the flow enters the gap and how much goes over the body.

4. Computational results.

Numerical solutions for the constant-curvature-underbody case are produced using a fourth-order Runge Kutta method. The system of equations (3.3d), (3.10b) and (3.13b) are solved simultaneously to understand the evolution of $\bar{\theta}, \bar{K}_{\bar{h}}$ and \bar{p}^+ over time. The solution presented in figure 3 is the case where the initial conditions are $\bar{\theta}(0) = -1, \dot{\bar{\theta}}(0) = -1, \bar{K}_{\bar{h}}(0) = 1, \bar{h}(0) = 0, \dot{\bar{h}}(0) = 0, I = 1, M = 5I, b = 1, \beta = 1/2$ and $\bar{D} = 1, \lambda = 1$ (without loss of generality $\bar{D} = 1, \lambda = 1$ for all scenarios in the present downstream-moving wall configurations, in contrast with upstream-moving wall configurations which are addressed later in section 6). Subsequent computational studies will use these initial conditions with any changes to the input parameters stated. Moreover time \bar{T} is written as t for convenience in our figures and $K_{\bar{h}}, \theta, p$ stand for $\bar{K}_{\bar{h}}, \bar{\theta}, \bar{p}^+$ respectively.

After an initial positive increase, the pressure $\overline{p^+}$ decreases until $t = 12$, reaching a negative stagnation point/minimum. A clockwise rotation is induced in the body position, increasing $\bar{\theta}$ in the negative direction, whilst for the fluid motion, after initially falling, $\bar{K}_{\bar{h}}$ begins to increase steadily, peaking at $t = 12$. The trend in $\bar{K}_{\bar{h}}$ roughly mirrors that of θ . Accordingly, as the pressure begins to increase, after $t = 12$ rotation of the body reverses and $\bar{K}_{\bar{h}}$ begins to fall. Notably, finite time break-up (FTBU) occurs or at least is suggested after $t = 25$ with the pressure falling rapidly and both $\bar{\theta}$ and $\bar{K}_{\bar{h}}$ increasing sharply.

Regarding the slip velocity about the body, flow reversal is seen across the body length. At the trailing edge, $X = 1$, the positive slip velocity mirrors the behaviour at the leading edge. At the middle of the body, after an initial positive velocity, a slip velocity of zero is maintained until $t = 24$. At the leading edge, $X = 0$, the body initially experiences a positive slip velocity which quickly becomes negative. In line with the flow progression seen above, the velocity decreases until $t = 12$, increasing back to zero thereafter. The flow again reverses to positive, with each velocity becoming equal, as the FTBU takes over around $t = 25$.

Considering this example behaviour, of particular interest is the effect that changes in body curvature b and the moment of inertia I has on the FTBU and the relationship between fluid body motion ($\bar{\theta}$), fluid motion ($\bar{K}_{\bar{h}}$) and the pressure conditions ($\overline{p^+}$).

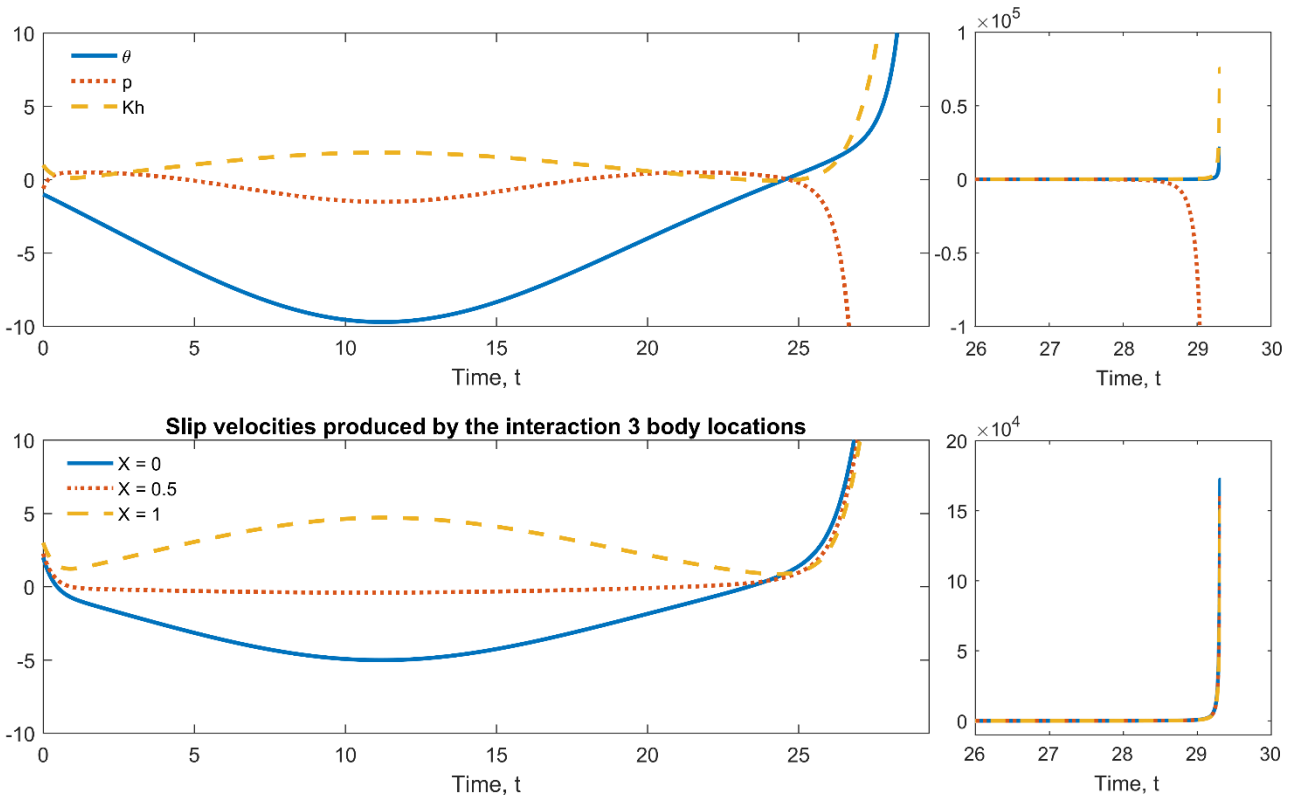


Figure 3: Evolution of the coupled fluid-body motion for a particle with constant curved underbody of $b = 1$ and moment of inertia $I = 1$, and mass $M = 5I$. The body begins with an initial orientation of $\bar{\theta}(0) = -1$ and angular velocity $\dot{\bar{\theta}}(0) = -1$, submerged in a fluid with initial $\bar{K}_{\bar{h}} = 1$. The progression of the slip velocities about the body is also presented, showing flow reversal across the submerged body.

4.1. Varying the body curvature parameter b .

The body parameter may be varied both positively and negatively, inducing different responses in the flow-body motion and different behaviour thresholds. In figure 3, where $b = 1$, the apparent FTBU began to occur after $t = 25$. In the scenarios shown in figure 4 the body parameter is varied slightly to show how the evolution of the system changes for values of b about 0. As shown, decreasing b leads to the time until

FTBU increasing. Otherwise the system continues to behave in a dynamically similar fashion for $\bar{\theta}$, \bar{p}^+ and $\bar{K}_{\bar{h}}$.

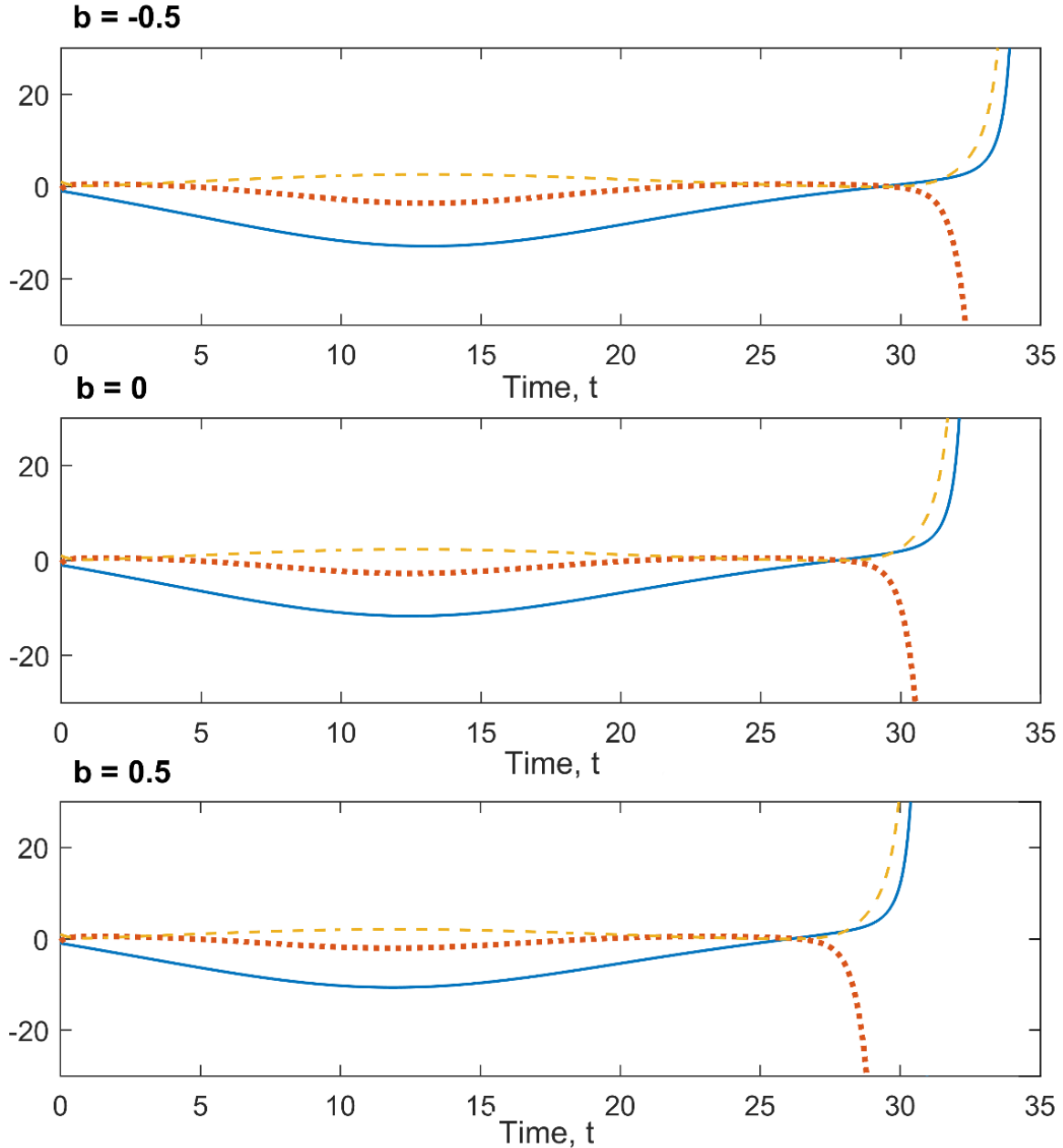


Figure 4: Evolution of the coupled fluid-body motion for a particle with curved underbody of $b = -0.5, 0$ and 0.5 . $\bar{\theta}$, solid line; \bar{p}^+ , dotted line; $\bar{K}_{\bar{h}}$, dashed line.

Continuing for large negative body curvature, figure 5 presents results for $b = -1, -10, -100$ and -200 . For $b = -1$, the trend of increasing time to FTBU is seen. In each of the other solutions, the system dynamics change significantly. At some value $b = b_{\pm}^+$, $-1 > b_{\pm}^+ > -10$, the FTBU behaviour no longer occurs over the short time frame with the body's response and fluid motion now becoming increasingly oscillatory with greater amplitude and frequency (numerical investigation found $b_{\pm}^+ \approx -2.5$ for the given initial conditions). For $b < b_{\pm}^+$, $\bar{p}^+ < 0$ and $\bar{\theta} < 0$ throughout the solution, and \bar{p}^+ now achieves minimal values that are far less than the minimum of $\bar{\theta}$.

The dynamics for positively increasing body curvature are presented in figure 6 for $b = 1, 10, 100$ and 200 . Unlike the behaviour seen in figure 5, as b increases the time to FTBU falls for values up to $b = 100$. As b increases further, at some value $b = b_{\pm}^+ > 100$, the dynamics again switch to an oscillatory response in the both the body motion and fluid motion (numerical investigation found $b_{\pm}^+ \sim 101$ for the given initial

conditions). Notably, for $b > b_+^+$ the behaviour of the oscillatory system differs from the $b < b_+^+$ scenario as $\overline{p^+}$ may now take positive values. Additionally, the $\bar{\theta}$ response is now out of phase with the $\overline{p^+}$ response.

To investigate further, slip velocities across the body for $b = 200$ and $b = -200$ are shown in figure 7. For $b = 200$, the slip velocity at $X = 0$ and $X = 1$ oscillates taking positive values and proceeding slightly out of phase with one another. Notably, there is only a small difference between the two solutions. However, the slip velocity at $X = 0.5$ shows significant flow reversal, portraying a comparatively large and negative response. For $b = -200$ a very different response occurs. The slip velocity at the leading edge and trailing edge now mirror one another, as in figure 3, oscillating at a similar frequency and magnitude. For $X = 0.5$ the slip velocity oscillates about small positive values over the computed interval.

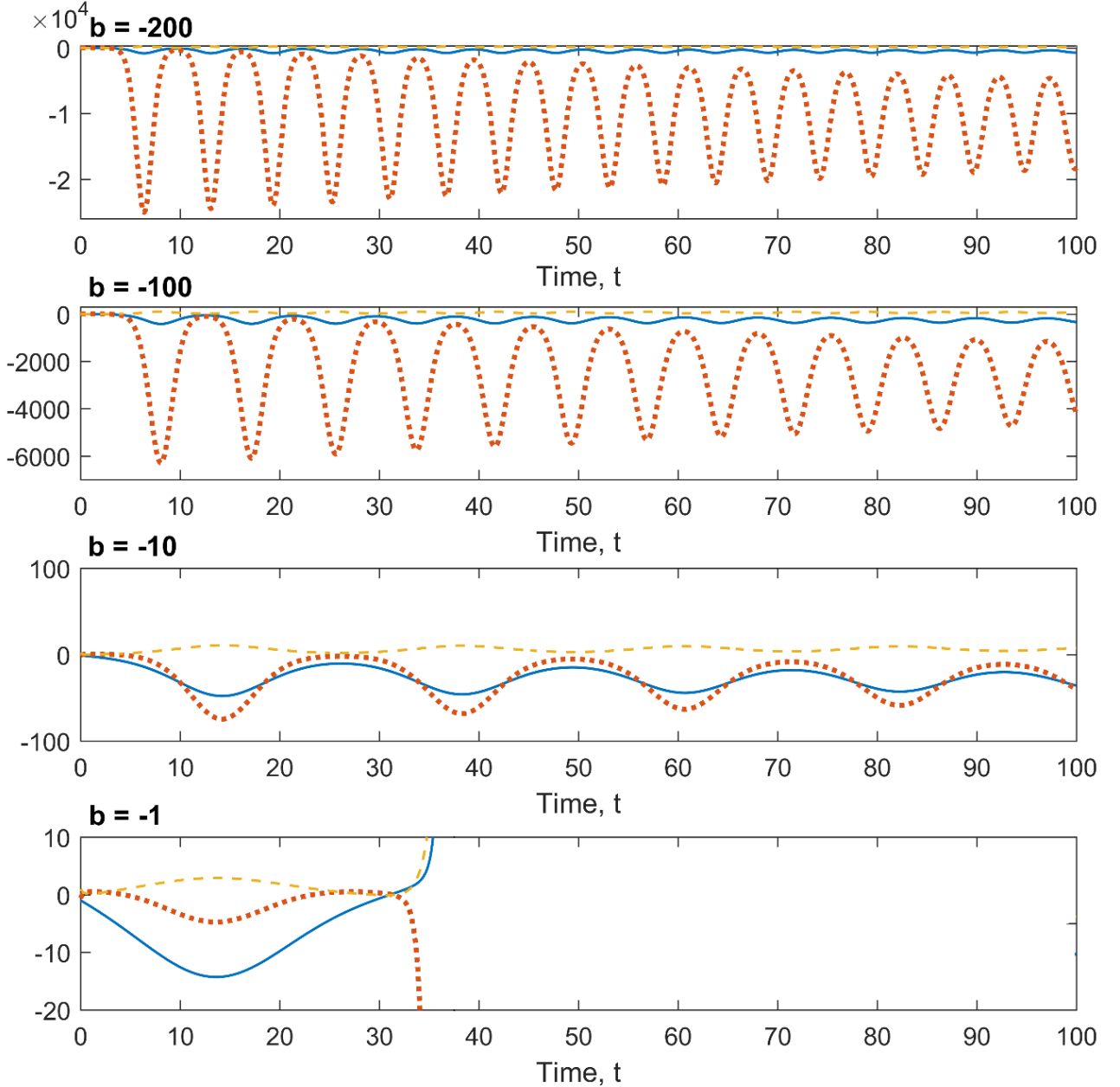


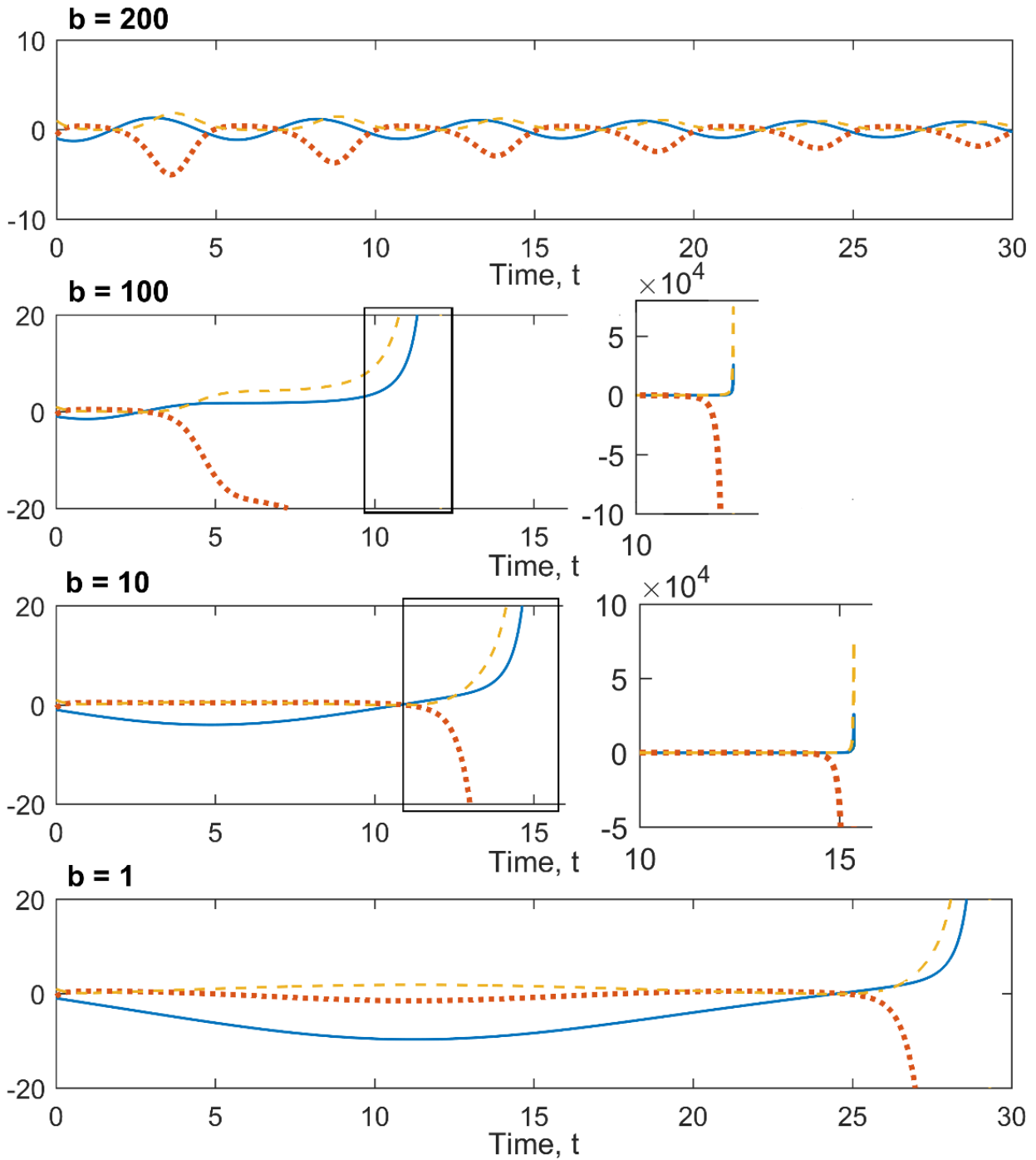
Figure 5: Evolution of the coupled fluid-body motion for a particle with curved underbody of $b = -200$, -100 , -10 and -1 . $\bar{\theta}$, solid line; $\overline{p^+}$, dotted line; $\overline{K_r}$, dashed line.

4.2. Varying the moment of inertia I .

The moment of inertia I is now varied positively for large and small values. In figure 8, with $b = 1$, increasing I greatly increases the time to FTBU in a manner similar to initially varying b . In comparison, as I becomes larger the magnitude of the pressure response increases, maintaining a negative value

throughout. For some value of I , its minimum value becomes significantly lower than the minimum $\bar{\theta}$ response.

Figure 6: Evolution of the coupled fluid-body motion for a particle with curved underbody of $b =$



200, 100, 10 and 1. $\bar{\theta}$, solid line; \bar{p}^+ , dotted line; $\bar{K}_{\bar{h}}$, dashed line.

In figure 9, again with $b = 1$, I is decreased to $I = 0.0005, 0.001, 0.02$ and 0.025 . For $I = 0.0005, 0.001$ and 0.02 both \bar{p}^+ and $\bar{K}_{\bar{h}}$ have a small initial oscillation, which quickly settles to 0. In these cases, the body begins to rotate with $\bar{\theta}$ progressing as a damped wave, eventually settling to a constant orientation. The system then runs in a steady state. For $I = 0.025$, the wave response is still seen, however its frequency has greatly reduced. Further increases in I subsequently result in the FTBU behaviour.

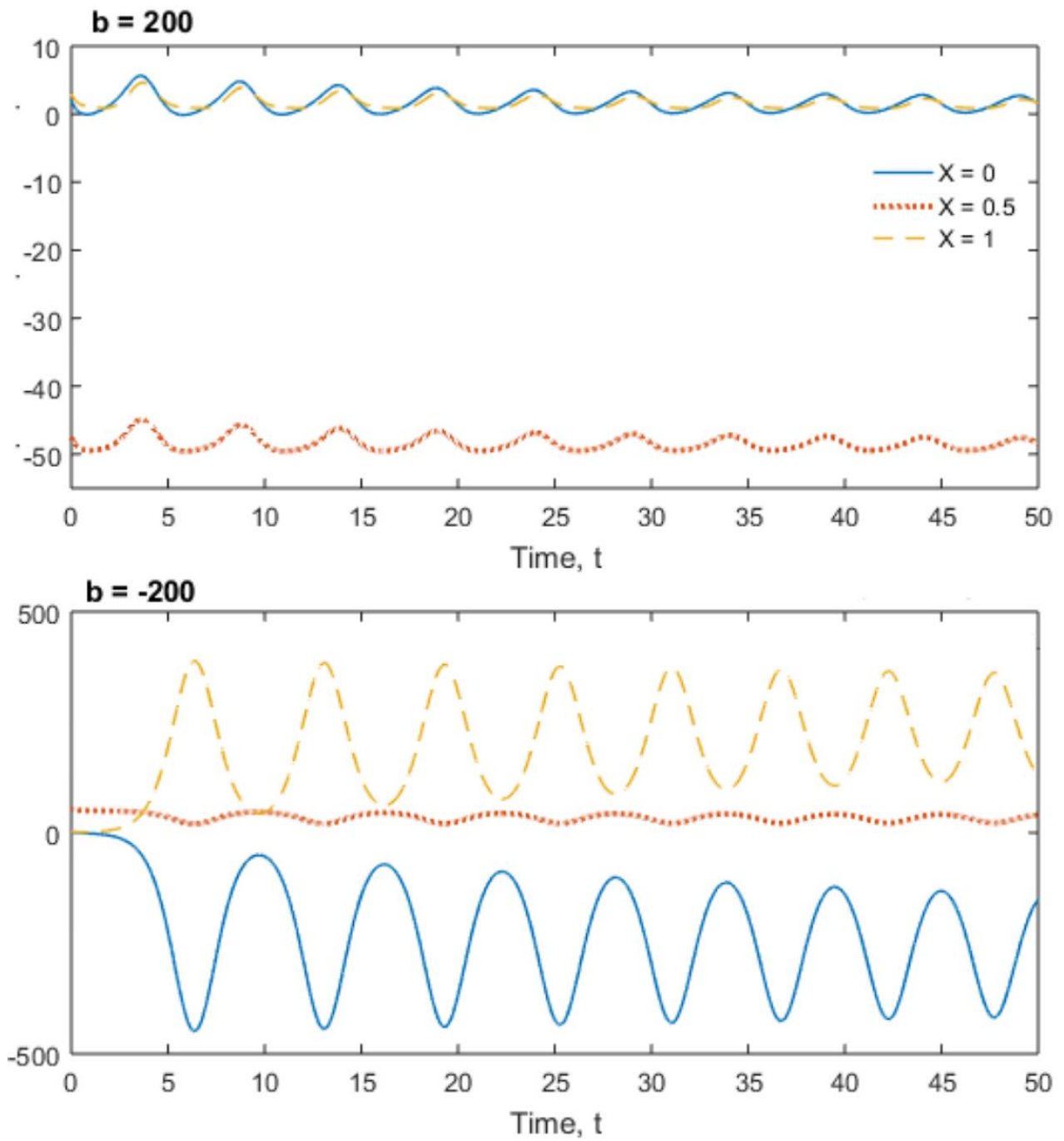


Figure 7: Evolution of the slip velocities about the body at $X = 0, 0.5$ and 1 are presented showing different flow reversal behaviour across the submerged particle for $b = 200$ and $b = -200$. $X = 0$, solid line; $X = 0.5$, dotted line; $X = 1$, dashed line.

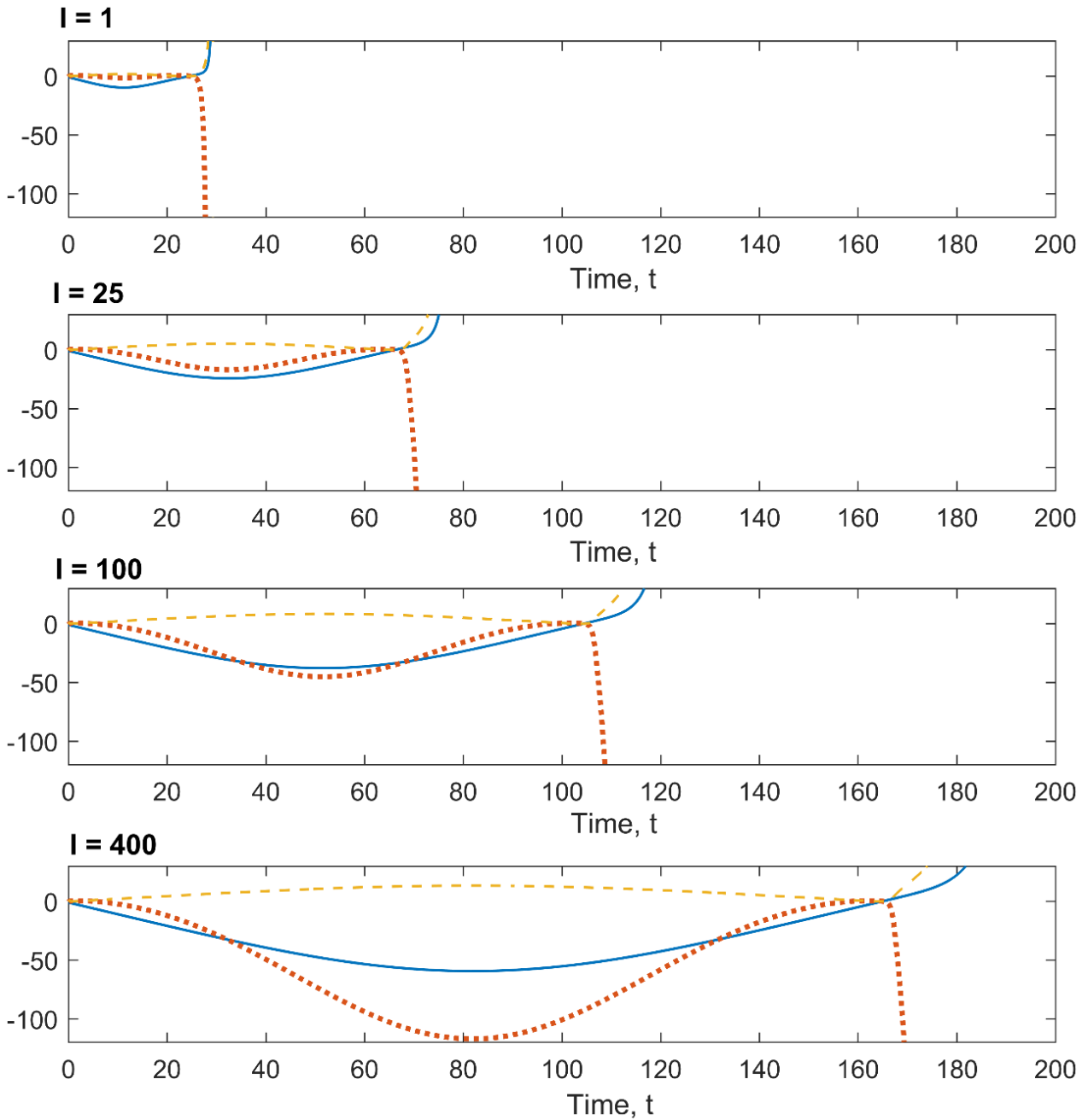


Figure 8: Evolution of the coupled fluid-body motion for a particle with inertia value $I = 1, 25, 100$ and 400 . $\bar{\theta}$, solid line; \bar{p}^+ , dotted line; $\bar{K}_{\bar{h}}$, dashed line.

4.3. Influence of the centre-of-mass position.

The effect of changing the centre of mass (COM) on the fluid-body motion is shown in figure 10. Shifting the centre of mass to the extremities of the particle, using the initial conditions for the case shown in figure 3, changes the time until FTBU. As the COM is moved to the leading edge, $X = 0$ and $\beta = 0.01$, the time to FTBU falls, whilst moving it towards the trailing edge, $X = 1$ and $\beta = 0.99$, the time increases. Otherwise, the system continues to behave in a dynamically similar fashion for $\bar{\theta}$, \bar{p}^+ and $\bar{K}_{\bar{h}}$ for the given initial conditions.

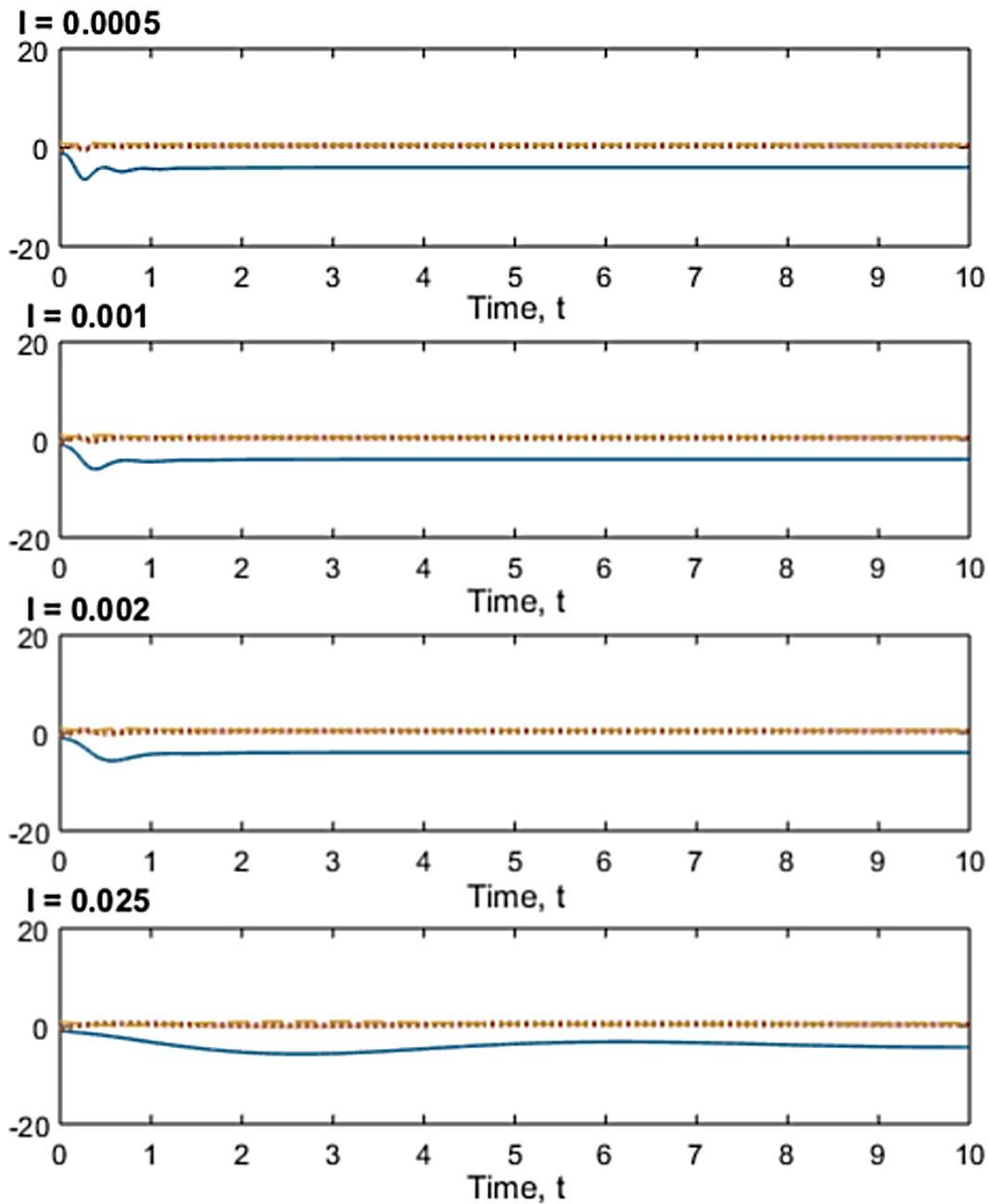


Figure 9: Evolution of the coupled fluid-body motion for a particle with inertia value $I = 0.0005, 0.001, 0.002$ and 0.025 . $\bar{\theta}$, solid line; \bar{p}^+ , dotted line; \bar{K}_n , dashed line.

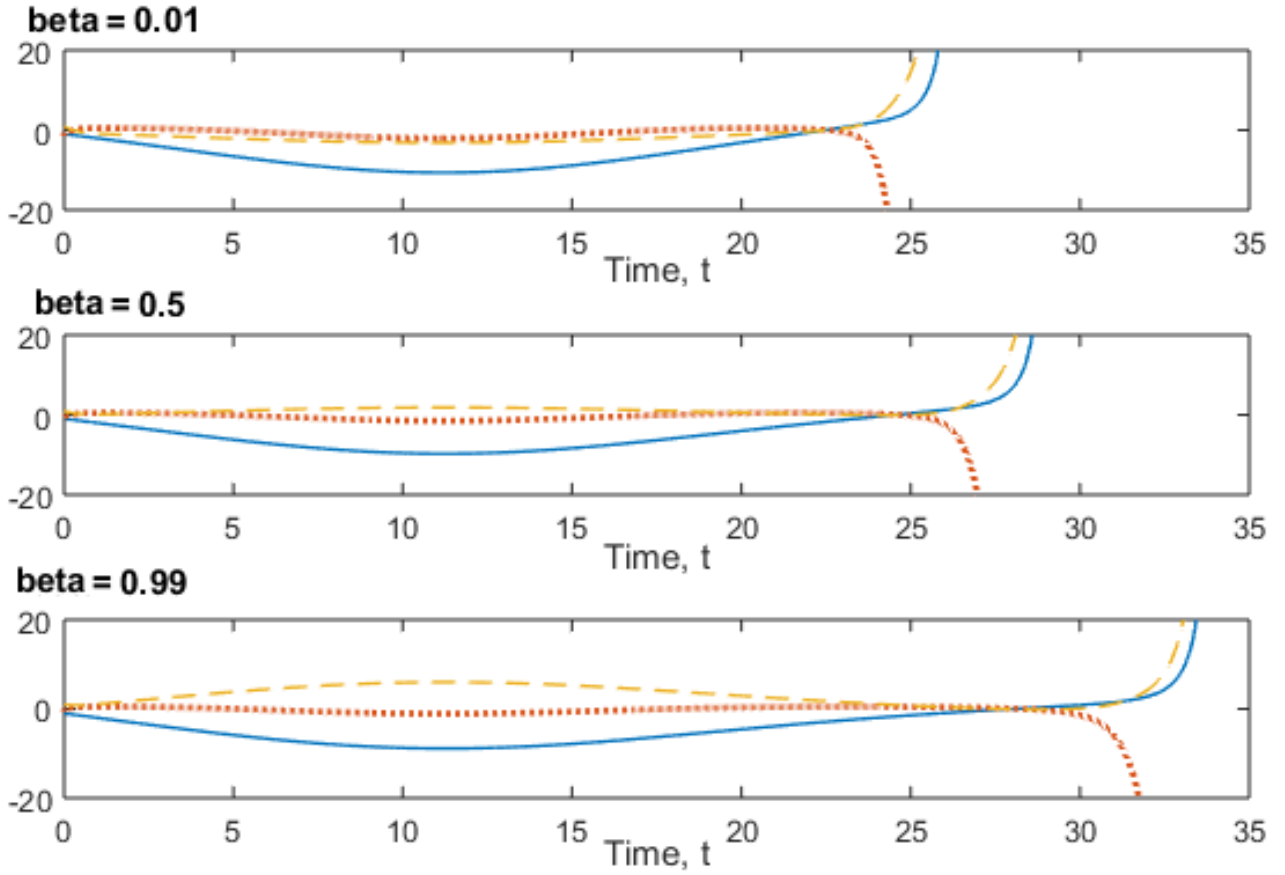


Figure 10: Evolution of the coupled fluid-body motion for a particle with a shifted centre of mass, $\beta = 0.01, 0.25, 0.5, 0.75$ and 0.99 . $\bar{\theta}$, solid line; \bar{p}^+ , dotted line; $\bar{K}_{\bar{h}}$, dashed line.

To further understand the dynamics highlighted in the above numerical study, analytical results are now sought, presented in section 5

5. Analysing parametric effects.

Analytical features are also of much interest and shed light on the interactive properties concerning finite-time blow-ups, limit cycles, extreme values of the governing parameters and initial conditions, as follows.

5.1. Large-amplitude blowup or limit cycles.

Although limit cycles are clearly possible in certain regimes, a singular response at finite time seems a quite common occurrence across much of the parameter space according to the computational work above. This finite-time blowup at some time $\bar{T} = \bar{T}_0$ – say has the analytical form:

$$(\bar{K}_{\bar{h}}, \bar{\theta}, \bar{D}^+) = (\bar{T}_0 - \bar{T})^{-2} (K_1, \theta_1, D_1^+) + \dots, \quad \bar{p}^+ = (\bar{T}_0 - \bar{T})^{-4} p_1^+ + \dots, \quad (5.1)$$

implied by the orders of magnitude present in the system (3.3d), (3.10b) and (3.13b). Substitution of (5.1) into that system leads to the following balances being obtained between the coefficients,

$$72 I = \lambda (\lambda K_1 \pm D_1^+), \quad (5.2a)$$

$$(\lambda K_1 \pm D_1^+) \theta_1 = -\frac{p_1^+}{\lambda}, \quad (5.2b)$$

$$K_1 = -\frac{\theta_1}{2} \pm \frac{D_1^+}{\lambda}, \quad (5.2c)$$

along with D_1^+ being the positive square root of $-2p_1^+$. It is notable that among the time derivatives present in the original system only the double time derivative multiplying the moment of inertia I affects the

balance in (5.2a-c). It follows from the above balance that the possible values of the coefficient D_1^+ are found to be

$$D_1^+ = 288 \left(s_1 \pm \frac{3^{1/2}}{2} \right) \frac{I}{\lambda}. \quad (5.3)$$

Here $s_1 = \pm 1$ nominally but the requirement of positive D_1^+ allows only the value $s_1 = 1$. From the above it then follows that the results

$$K_1 = -72 (3^{1/2} \pm 2) 3^{1/2} \frac{I}{\lambda^2}, \quad \theta_1 = 144 (7 \pm (4)3^{1/2}) \frac{I}{\lambda^2}, \quad p_1^+ = -\frac{D_1^+}{2} I^2, \quad (5.4a-c)$$

apply for the other coefficients in (5.1). The asymptotic behaviour in (5.1) appears to explain well the singular-looking trends seen in the numerical results of the previous section, while the fact that $\theta_1, -p_1^+$ must be positive from (5.4b, c) whereas K_1 may be positive or negative is also in line with the numerical findings.

The physical mechanism driving the breakup is based on a self-sustaining nonlinear interaction between the body motion and the fluid motion. The scaled pressure is approximately $-1/2$ (*speed*)² from the fluid momentum in (3.5b) as well as from the Bernoulli property. The speed however is proportional to the variation in displacement or the scaled angle θ from (3.5e) with (3.3c). Hence a pressure proportional to $-1/2 \theta^2$ is provoked. This pressure then acts over the whole under-surface of the body to give a moment force proportional to θ^2 as far as the body movement is concerned. So the body motion involves a balance between the rotational mass-acceleration, proportional to the second derivative of the angle θ with respect to time, and the pressure force which is proportional to θ^2 . The balance implies a θ response going like the -2 power of time, $(\bar{T}_0 - \bar{T})$. This agrees with the asymptotic result for the scaled angle in (5.1). The coefficients in (5.4a-c) stem from the details of the pressure force on the body. The pressure itself goes like the -4 power of $(\bar{T}_0 - \bar{T})$ because of the θ^2 feature above. Further, the blowup is independent of the body-curvature parameter b and so can occur for any value of b whether positive or negative and it can also occur for any moment-of-inertia factor I since the latter has to be positive.

5.2. Small amplitudes.

The behaviour at small amplitudes can be shown to match with that in [7] as mentioned earlier.

5.3. Varying b and I .

The effects of varying the body-shape parameter b and the scaled moment of inertia I warrant consideration. When b is large and positive for example assuming $\bar{p}^+, \bar{\theta}$ and $\bar{K}_{\bar{h}}$ remain of mild size and other parameters are of order unity we find that the leading terms of $O(b^2)$ in the right-hand side of (3.13b) cancel out but the $O(b)$ terms are nonzero. Hence predominantly the equation

$$2 I \frac{d^2 \bar{\theta}}{d\bar{T}^2} = -\frac{\lambda^2 b \bar{\theta}}{60}, \quad (5.5a)$$

holds, giving oscillations. This also implies that the time scale is short and the scaled oscillation frequency ω (say) is large,

$$\bar{T} = O\left(b^{-\frac{1}{2}}\right), \quad \omega = \lambda \left[\frac{b}{120 I} \right]^{1/2}, \quad (5.5b)$$

from the balance in (5.5a). The predictions in (5.5b) are seen to be close to the computational results for b large and positive. The high-frequency behaviour here is physically in keeping with the high curvature of the body.

When b is large and negative, on the other hand, large oscillations are obtained and the relevant time scale becomes small of order $|b|^{-1/2}$, while the relevant expansion of the interactive solution turns out to be

$$(\bar{K}_{\bar{h}}, \bar{\theta}, \bar{p}^+, \bar{D}^+) = (|b|K_2, |b|\theta_2, |b|p_2^+, |b|D_2^+) + \dots \quad (5.6a)$$

Substitution into the system (3.3d), (3.10b) and (3.13b) then yields the following governing equations at leading orders, respectively,

$$12I \frac{d^2 \theta_2}{d\bar{T}^2} = \lambda^2 \left(-\phi_2 + \frac{1}{10} \right) \theta_2, \quad (5.6b)$$

$$(\lambda K_2 \pm D_2^+) \theta_2 = -\frac{p_2^+}{\lambda}, \quad (5.6c)$$

$$K_2 = -\frac{\theta_2}{2} \pm \frac{D_2^+}{\lambda}, \quad (5.6d)$$

where $\phi_2 = -(K_2 \pm D_2^+/\lambda)$, $D_2^+ = (-2p_2^+)^{1/2}$ and $\bar{T} = |b|^{-1/2} \tilde{T}$ with \tilde{T} of $O(1)$. This system can be manipulated into the relatively simple nonlinear form of an equation involving θ_2 alone,

$$\left(\frac{d\theta_2}{d\bar{T}} \right)^2 = (a_2 \theta_2^3 + b_2 \theta_2^2 + c_2) \frac{\lambda^2}{I}, \quad (5.6e)$$

where c_2 is an arbitrary constant of integration (determined by the initial conditions). The known constants $a_2 = (7 \pm (4)3^{1/2})/36$ and $b_2 = 1/120$ are positive. When c_2 is positive the reduced system thus admits nonlinear periodic solutions for a finite range of negative values of θ_2 , in keeping with the oscillations seen in the numerical solutions. (Comparing further, we see that for the computed case of b equal to -100 the values of $\bar{\theta}$ are always negative, as the analysis suggests, and when $\bar{\theta}$ is at a minimum of about -400 the analysis implies a \bar{p}^+ value of $-1/2 E^2$, giving $-5,600$ approximately. That is not far from the computed values of \bar{p}^+ . The latter values are varying slowly with time whereas the main period is short and quite possibly of the order $|b|^{-1/2}$ suggested by the analysis.) Outside the above range, the system admits a finite-time blowup whereby θ_2 tends to ∞ owing to the nonlinear contribution involving a_2 in (5.6e), in a form identical with that in (5.1). Again, the high-frequency behaviour arising here for given high curvature of the body appears to make good sense dynamically.

For small values of b the solution appears to be a regular perturbation from the form holding when b is zero.

When I is large and positive, the typical range of interest has $(\bar{K}_h, \bar{\theta}, \bar{p}^+)$ of order unity and slow evolution in the sense that $\bar{T} = I^{1/2} \hat{T}$. This slowness in response is physically sensible for such a relatively large moment of inertia. In this case the single derivatives with respect to time in π_1, π_2 and (3.10b) become negligible and so we are led to two equations controlling $\bar{\theta}, \bar{D}^+$, namely

$$24 \frac{d^2 \bar{\theta}}{d\hat{T}^2} = \bar{D}^{+2} - 1 - \frac{b\bar{\theta}}{5}, \quad (5.7a)$$

$$\left(\pm 2\bar{D}^+ - 1 - \frac{\bar{\theta}}{2} \right) \bar{\theta} = \frac{\bar{D}^{+2} - 1}{2}. \quad (5.7b)$$

Here λ, \bar{D} are normalized to unity and \bar{p}^+ is given by $(1 - \bar{D}^{+2})/2$. The nonlinear pair (5.7a, b) may be integrated with respect to \hat{T} in principle to provide an energy-like equation for $(d\bar{\theta}/d\hat{T})^2$ as in (5.6e). Limit cycles and finite-time blowups remain the possible end-states of the system here; the blowup properties (5.1)-(5.4c) can be checked as being present still in this simpler system. Computational findings tend to agree with the asymptotic form here especially in terms of the slow time scale.

When I is small there is a similar physical effect in the sense that the representative time scale also becomes small. Thus the orders of magnitude

$$\bar{T} = O(I), \quad \bar{\theta} = O(I^{-1}), \quad (5.8)$$

are implied analytically by the balances in the governing equations. Numerical results appear to conform with the trend in (5.8).

5.4. Initial conditions.

The influence of the initial conditions is significant as well because they help to dictate whether the interactions develop eventually into periodic or quasi-periodic limit cycles or, rather, into blow-ups within a finite time. This influence is seen clearly in the computations of the previous section and also in the analytical results such as in (5.6e).

6. Discussion.

The present work has described through modelling, analysis and reduced computations the nonlinear effects and flow separations that can take place during a fluid/body interaction within a boundary layer. This is in the context of a single body translating near a solid surface and it appears to be a new development. Concerning main outcomes of the work, we find here that not all such bodies are likely to impact upon the wall; some oscillate. Additionally the quite common occurrence of a blowup within a finite scaled time implies a substantial change of amplitude in both the fluid and the body motions as follows. (We note in passing the relatively large numerical values of $|b|$ observed in some of the results, such as in figures 5, 6, and likewise for some of the coefficients such as in (5.4a-c), but these do not fundamentally disturb the asymptotic orders of magnitude addressed in section 3. Smaller-scale breakup of the thin viscous layers on the body and the wall is another interesting factor but seems unlikely in the presence of the increasingly positive slip velocities arising as the finite-time break-up of this article is approached: see in figure 3.)

The blowup trend in (5.1) forces the original small displacement contribution A_1 in (3.1a) to grow like $(\bar{T}_0 - \bar{T})^{-2}$ as \bar{T} tends to the finite time \bar{T}_0 , since A_1 depends linearly on $\bar{K}_{\bar{h}}$ and $\bar{\theta}$ and both of these are singular as in (5.1). Moreover \bar{D}^+ exhibits the same growth in (5.1) and thus adds to the $(\bar{T}_0 - \bar{T})^{-2}$ enhancement of the originally small $O(\varepsilon)$ term on the right-hand side in (3.1a). Therefore that term overtakes the first $O(1)$ term u_0 when $\bar{T} - \bar{T}_0$ decreases to the order $\varepsilon^{1/2}$. At that stage the pressure response also rises considerably, having begun small of $O(\varepsilon^2)$ in (3.1c) but growing as $(\bar{T}_0 - \bar{T})^{-4}$ by virtue of (5.1) and hence becoming of $O(1)$. The consequence of these relatively rapid growths is that the interaction process becomes fully nonlinear at a time given by $T = \varepsilon^{-1} \bar{T}_0 + O(\varepsilon^{-1/2})$, with the complete system of (2.1a)-(2.2f) then being set into action, despite the small amplitude of the initial disturbance in (3.1). An important point for future study, however, is that the fluid flow becomes quasi-steady then and the body-motion unsteadiness dominates. We should comment further that acceleration and inertial effects dominate throughout and lubrication effects are negligible in all of these settings. The overall emphasis has been on the understanding of possible mechanisms in play when a body enters a boundary layer. On the other hand, there is the issue of whether the study or this type of study provides useful insight for practical advances; that remains to be seen.

When the body is translating downstream relative to the wall the given constant $u_c = C$ is positive. In the reduced-body-speed case C then becomes $\varepsilon \bar{C}$. A simple replacement of \bar{D} by $-\bar{C}$ applies through the whole system (3.3d), (3.10b), (3.13b), including replacing $-\bar{D}$ by $+\bar{C}$ in (3.3d), and, following this, we can normalise \bar{C} to be unity without loss of generality. Hence effectively we can just set $\bar{D} = -1$ in the system. This formally yields the sample result in figure 11. Our initial concentration in this paper on negative u_c , where D, \bar{D} are positive, is due to the fact that the downstream-moving wall in combination with forward flow would allow a laminar boundary layer to stay attached. The sublayers of concern here are unsteady ones however and so may remain attached for a finite time in line with the evolving flow found outside the sublayer. Turbulent sublayers also tend to remain attached. In addition it is helpful to consider the flow induced in the Euler zone. When D is positive then totally forward flow can hold in that zone at those times when the downstream flow (with $+D^+$ present) is also forward and this is subject to an adverse or favourable pressure gradient depending on whether the incremental pressure p^+ is positive or negative respectively. When D is positive but the downstream flow (having $-D^+$) is reversed then a stagnation point occurs on the wall. When C is positive corresponding to reversed incident motion and the downstream flow (with $+D^+$) is forward then again a stagnation point occurs on the wall. When C is positive but the downstream flow (with $-D^+$) is also reversed then we expect that no stagnation point occurs on the wall,

the flow there being completely reversed throughout the Euler zone. The second scenario here yields effectively a rear stagnation point on the wall and this is the most likely to promote secondary separation, depending on whether the sublayer motion is laminar or turbulent, whereas the third scenario induces effectively a front stagnation point and no secondary separation. Some finer details of the viscous laminar or turbulent sublayers close to the solid surface here and in earlier results are evident in [15-18].

Future work in the area has many different aspects to explore. For the current boundary-layer setting the effects of a number of bodies stacked normally above each other, essentially in parallel, is of concern. It is equivalent to the formulation in [1] but with nonzero vorticity present now, and the occurrences of clashes in this case would be interesting to investigate. Whether bodies placed in series can readily be treated theoretically is unknown as yet. There is also the alternative setting of channel flow, where the original problem (2.1)-(2.4b) largely remains intact for a single body. Returning to the important influence of nonlinearity, we note that the fully nonlinear regime delineated in section 2 is of much interest. As well as the possibility of a clash between bodies as in [1] a clash with the underlying solid wall may induce further separations. Also of concern are the effects of nonlinearity in the configurations of [6, 7] where the body velocity relative to the wall is negligible. Above all perhaps interactions in three spatial dimensions and with more bodies present need much further consideration.

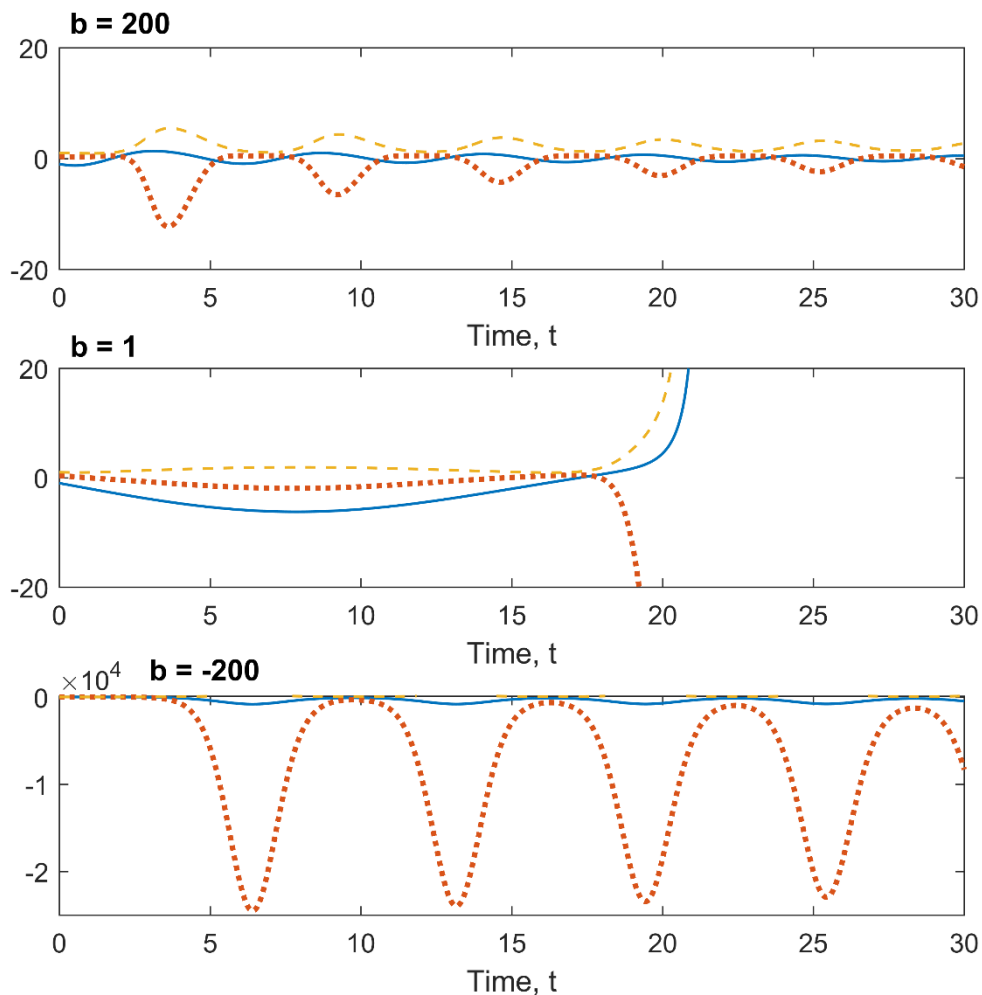


Figure 11: Evolution of the coupled fluid-body motion for a particle with $\bar{D} = -1$; thus the body is translating downstream relative to the wall. The body begins with the same initial conditions as in figure 3. $\bar{\theta}$, solid line; \bar{p}^+ , dotted line; \bar{K}_h , dashed line.

7. Conclusions.

Given the motivating examples within the hydrodynamics of ice, the findings from this work provide some key insights that have not been covered within previous studies. In particular, they suggest that several underlying mechanisms are important within the noted fluid-body scenarios. The effects of nonlinearity form an important element in the understanding and prediction of body movement in a sheared fluid flow such as the presently studied boundary-layer flow. The presented work is believed to be the first such nonlinear analysis-based study, addressing fairly low-amplitude but nonlinear interactions between the fluid flow and the body motion and so contrasting with linearized theories developed in recent works. This allows separation in the sense of flow reversal to be included in the evolution of the combined body and fluid motion, separation being another physically important element in practice.

The model interaction leads to two main outcomes: a blowup singularity after a finite scaled time or continuing nonlinear oscillations. Transient separations occur in many cases, although the finite-time blowup scenario is separation-free. The dynamics involved here at high Reynolds number is predominantly inviscid, as previous viscous-inviscid theory suggested, and it is also assumed that the body is thin. In many cases the thin body seems destined to impact upon the wall eventually or to continue to fly away from the wall, thereby exiting the boundary layer, but not all cases do so; some seem destined to remain fluctuating within the boundary-layer flow until further physical effects come into play.

The various influences from the scaled moment of inertia of the body, the body shape and the position of the centre of mass have been examined. The scaled mass of the body plays only a secondary role as far as the dynamic fluid /body interaction is concerned in the current nonlinear regime. Upstream and downstream translation of the body relative to the solid wall underneath the boundary layer has also been incorporated. It is interesting that the finite-time blowup discovered here is independent of the direction of that translation, a feature which needs further investigation for more highly nonlinear situations. This blowup is also unaffected by several other factors, such as the detailed body shape.

Finally, this work is of scientific and industrial benefit for the hydrodynamic modelling of ice. It indicates both that several important physical phenomena and dynamics should be considered when modelling scenarios as suggested in the Introduction (and thus converted into industrially applicable methods), and that further investigation is required to continue to understand better the wide range of scenarios that such fluid-body systems represent. Moreover, these detailed findings and explorations of parameter space are intended for use in increasing the understanding of ice-particle behaviour and consequent hazards near vehicles in motion.

Acknowledgements.

This work was supported by EPSRC [EP/R511638/1]. The authors thank AeroTex UK LLP for their continued input and insight in developing this work (through Richard Moser, Ian Roberts and Colin Hatch) and their joint financial support of RP. The authors also thank other colleagues for their interest and help, and thank UCL for support (IAA). Very helpful comments from the referees are acknowledged with gratitude.

Appendix A.

The Euler jump when the body speed is $O(1)$ or small.

For general body velocity u_c we have from (2.4a,c) the jump relation

$$Y = \int_0^Z [u_0(\eta) + D][(u_0(\eta) + D)^2 - 2p^+]^{-1/2} d\eta + Y_0, \quad (\text{A1})$$

between the velocity profiles on either side of the leading edge region. Here $u_c = -D$ and we recall $u_0(Y)$ is the original no-slip profile of the boundary layer; z is used as a marker upstream of the leading edge for arguments regarding streamlines. In terms of infinitesimal increments, immediately downstream of the leading edge $dY = d\psi/w_0^+(Y)$, which traced back upstream is $d\psi/[w_0(z)^2 - 2p^+]^{1/2}$ on the same streamline and so gives $w_0(z)dz/[w_0(z)^2 - 2p^+]^{1/2}$. This coupled with $u_0 + D = w_0$ confirms the result

(A1). The result applies with Y_0 zero for completely forward flow whereas in the presence of reversed flow the dividing streamline height Y_0 is added as in (A1).

When D is small the pressure p^+ is expected to be small also, such that $D = \varepsilon \bar{D}$ and $p^+ = \varepsilon^2 \bar{p}^+$ to leading order, where $\bar{p}^+ < \frac{1}{2} (\bar{D})^2$. Then two tiers in Y emerge. First, near the wall $Y = \varepsilon \bar{Y}$, the corresponding $z = \varepsilon \bar{z}$ and so $u_0(z) = \lambda \varepsilon \bar{z} + O(\varepsilon^2)$ gives uniform shear flow as the leading approximation. Hence (A1) gives to leading order

$$Y = \varepsilon \bar{Y} = \varepsilon \lambda^{-1} \{ [(\lambda \bar{z} + \bar{D})^2 - 2 \bar{p}^+]^{1/2} - \bar{D}^+ \} + \varepsilon \bar{Y}_0. \quad (\text{A2})$$

If the flow is partially reversed the expectation is that $Y_0 = \varepsilon \bar{Y}_0$ predominantly and so the contribution $\varepsilon \bar{Y}_0$ is added on the right in (A2). As a check, Y is zero at the wall when Y_0 is zero. On the other hand at large \bar{z} and \bar{Y} values (A2) gives

$$\bar{Y} \sim \lambda^{-1} \{ \lambda \bar{z} + E^+ + O(1/\bar{z}) \} + \bar{Y}_0, \quad \text{with } E^+ = \bar{D} - \bar{D}^+, \quad (\text{A3})$$

where E^+ acts as a displacement effect. Second, in the bulk of the flow Y is $O(1)$ and there (A1) leads to the relation

$$Y = z + \varepsilon \lambda^{-1} E^+ + \varepsilon \bar{Y}_0 + O(\varepsilon^2) \quad (\text{A4})$$

which matches with (A3). The result (A4) agrees well with the full computational values in figure 2 at small D values. The bulk thus feels only a uniform $O(\varepsilon)$ displacement of the original velocity profile. Accompanying this is an $O(\varepsilon^2)$ change in pressure; the dependence between displacement (proportional to E^+) and pressure (proportional to p^+) at $X = 0_+$ is as displayed in the second equation of (A3), given that $\bar{D}^+ = (\bar{D}^2 - 2 \bar{p}^+)^{1/2}$. The value of \bar{Y}_0 is either zero for forward flow or, for reversed cases, $2 \bar{D}^+ / \lambda$ according to section 2's final paragraph.

From the above we can determine the $Y(z)$ dependence across the leading edge Euler region. Additionally we know $\psi(z)$ there and hence we can find $Y(\psi)$, thence $\psi(Y)$ by inversion, and then obtain the corresponding velocity profile. Clearly a main effect however is the pressure-free displacement in the bulk such that

$$u = u_0(z + \varepsilon \lambda^{-1} E^+ + \varepsilon \bar{Y}_0) + \dots \quad u = u_0(z) + \varepsilon (\lambda^{-1} E^+ + \bar{Y}_0) u'_0(z), \quad (\text{A5})$$

is the velocity solution at $X = 0_+$ to $O(\varepsilon)$. This indicates that in terms of the main text

$$A_1(0_+, \bar{T}) = -(\lambda^{-1} E^+ + \bar{Y}_0). \quad (\text{A6})$$

Recall that E^+ , \bar{Y}_0 are time-dependent unknowns since \bar{p}^+ is: see (A3). See also below for an alternative derivation of (A5), (A6).

An alternative approach for the main result (A6) is as follows. The profile at $X = 0_-$ is given as $u_0(Y) + D$ with $u_0(Y) \sim \lambda Y$ near the wall and the incident pressure is taken as zero. To establish what the starting velocity profile is at $X = 0_+$, for the case $D \ll 1$ of interest where $D = \varepsilon \bar{D}$, we argue that in the sublayer where $Y = \varepsilon \bar{Y}$ we have

$$u = \varepsilon \lambda \bar{Y} + \varepsilon \bar{D}^+, \quad \text{at } X = 0_+. \quad (\text{A7})$$

This conserves vorticity there and gives the correct velocity at the wall, namely $\varepsilon \bar{D}^+$ where $\bar{D}^+ = (\bar{D}^2 - 2 \bar{p}^+)^{1/2}$ from Bernoulli. On the other hand in the region above that where Y is $O(1)$ three effects act together. The velocity profile at $X = 0_+$ is a pressure-free $O(\varepsilon)$ -displaced form of the incident profile, thus conserving vorticity along streamlines. Second, that incident profile is $u_0(Y) + \varepsilon \bar{D}$. Hence $u = u_0(Y + \varepsilon \bar{B}^+) + \varepsilon \bar{D} + \dots$ at $X = 0_+$ with \bar{B}^+ unknown; i.e.

$$u = u_0(Y) + \varepsilon \overline{B^+} u'_0(Y) + \varepsilon \overline{D} + \dots \text{ at } X = 0_+. \quad (\text{A8})$$

Third, matching at small Y requires the present region's $\lambda Y + \varepsilon \overline{B^+} \lambda + \varepsilon \overline{D} + \dots$ from (A8) to match with the sublayer's $\varepsilon \lambda \overline{Y} + \varepsilon \overline{D^+}$ from (A7). So we find that

$$\overline{B^+} \lambda = \overline{D^+} - \overline{D}. \quad (\text{A9})$$

The result (A9) agrees with (A6), i.e. it imposes $A_1(0_+, \overline{T}) = \lambda^{-1}(\overline{D^+} - \overline{D})$, which is the same as $-\lambda^{-1}E^+$. This yields the same results as before for the starting profile. We have considered the forward flow scenario but identical results apply for the partly reversed flow scenario with the minus sign on the square root holding then.

References

1. F T Smith and A S Ellis, On interaction between falling bodies and the surrounding fluid. *Mathematika*. 56 (2010) 140–168. <https://doi.org/10.1112/S0025579309000473>
2. P D Hicks and F T Smith, Skimming impacts and rebounds on shallow liquid layers, *Proc. Roy. Soc. A*. 467 (2011) 653–674. <https://doi.org/10.1098/rspa.2010.0303>
3. P L Wilson and F T Smith, Body-rock or lift-off in flow. *J Fluid Mech*. 735 (2013) 91–119. <https://doi.org/10.1017/jfm.2013.464>
4. F T Smith and K Liu, Flooding and sinking of an originally skimming body, *J Eng Math*. 107:1 (2017) 37–60. <https://doi.org/10.1007/s10665-017-9925-7>
5. F T Smith, S Balta, K Liu and E R Johnson, On dynamic interactions between body motion and fluid motion. Chapter in *Mathematics Applied to Engineering, Modelling, and Social Issues*. Pub Taylor & Francis. (2018)
6. F T Smith and E R Johnson, Movement of a finite body in channel flow, *Proc. Roy. Soc. A* 472:2191 (2016) 20160164. <https://doi.org/10.1098/rspa.2016.0164>
7. F T Smith, Free motion of a body in a boundary layer or channel flow, *J Fluid Mech*, (2017) 813:279–300. <https://doi.org/10.1017/jfm.2016.706>
8. Y Shao, M R Raupach, and P A Findlater, Effect of saltation bombardment on the entrainment of dust by wind, *J. Geophysical Research: Atmospheres* 98 (1993) 12719–12726. <https://doi.org/10.1029/93JD00396>
9. J M Foucaut and M Stanislas, Experimental study of saltating particle trajectories. *Experiments in Fluids* 22:4 (1997) 321–326. <https://doi.org/10.1007/s003480050054>
10. P Diplas, C L Dancey, A O Celik, M Valyrakis, K Greer, T Akar, The role of impulse on the initiation of particle movement under turbulent flow conditions, *Science* 322 (2008) 717–720. <https://doi.org/10.1126/science.1158954>
11. A J C Ladd, Numerical simulations of particulate suspensions via a discretized Boltzmann equation. Part 2. Numerical results. *J Fluid Mechanics*, 271 (1994) 311–339. <https://doi.org/10.1017/S0022112094001771>
12. B Willetts, Aeolian and fluvial grain transport. *Phil. Trans. Roy. Soc. A*, 356:1747 (1998) 2497–2513. <https://doi.org/10.1098/rsta.1998.0283>
13. V Loisel, M Abbas, O Masbernat and E Climen, The effect of neutrally buoyant finite-size particles on channel flows in the laminar-turbulent transition regime. *Phys Fluids* 25:12 (2013) 123304. <https://doi.org/10.1063/1.4848856>
14. C Schmidt and T M Young, The impact of freely suspended particles on laminar boundary layers. In *AIAA Aerosp. Sci. Mtg 5–8 Jan, Orlando, Florida, USA, AIAA* (2009). <https://doi.org/10.2514/6.2009-1621>
15. L Labraga, G Kahissim, L Keirsbulck, F Beaubert. An Experimental Investigation of the Separation Points on a Circular Rotating Cylinder in Cross Flow. *J. of Fluids Engineering* 129: 9 (2007) 1203–1211. <https://doi.org/10.1115/1.2746894>
16. A T Degani, F T Smith and J D A Walker, Unsteady separation past moving surfaces, *J Fluid Mech*, 375 (1998) 1–38. <https://doi.org/10.1017/S0022112098001839>

17. L L Van Dommelen and S F Shen, Boundary layer separation singularities for an upstream moving wall, *Acta Mechanica*, 49:3-4 (1983) 241-254. <https://doi.org/10.1007/BF01236354>
18. O Inoue, A numerical investigation of flow separation over moving walls. *J. Phys. Soc. of Japan* 50:3 (1981) 1002–1008. <https://doi.org/10.1143/JPSJ.50.1002>
19. F T Smith and O R Burggraf, On the development of large-sized short-scaled disturbances in boundary layers. *Proc. R. Soc. A* 399, (1985) 25-55. <https://doi.org/10.1098/rspa.1985.0046>